https://doi.org/10.5194/acp-2019-475
Preprint. Discussion started: 8 July 2019

Atmospheric Chemistry and Physics
Discussions
Open Access
EGU

Six Global Biomass Burning Emission Datasets: Inter-comparison and Application in one Global Aerosol Model

Xiaohua Pan[1,2,*] Charles Ichoku[3], Mian Chin[2], Huisheng Bian[4,2], Anton Darmenov[2], Peter Colarco[2], Luke Ellison[5,2], Tom Kucsera[6,2], Arlindo da Silva[2], Jun Wang[7], Tomohiro Oda[6,2], Ge Cui[7]

1. Earth System Science Interdisciplinary Center, University of Maryland, College Park, MD, USA
2. NASA Goddard Space Flight Center, Greenbelt, MD, USA
3. Howard University, Washington DC, USA
4. Joint Center for Earth Systems Technology, University of Maryland Baltimore City, Baltimore, MD, USA
5. Science Systems and Applications, Inc., Lanham, MD, USA
6. Universities Space Research Association, Columbia, MD, USA
7. University of Iowa, College of Engineering, Iowa City, IA, USA

* xpan333@umd.edu

Abstract

Aerosols from biomass burning (BB) emissions are poorly constrained in global and regional models, resulting in a high level of uncertainty in understanding their impacts. In this study, we compared six BB aerosol emission datasets for 2008 globally as well as in 14 sub-regions. The six BB emission datasets are: (1) GFED3.1 (Global Fire Emissions Database version 3.1); (2) GFED4s (Global Fire Emissions Database version 4 with small fires); (3) FINN1.5 (Fire INventory from NCAR version 1.5); (4) GFAS1.2 (Global Fire Assimilation System version 1.2); (5) FEER1.0 (Fire Energetics and Emissions Research version 1.0), and (6) QFED2.4 (Quick Fire Emissions Dataset version 2.4). Although biomass burning emissions of aerosols from these six BB emission datasets showed similar spatial distributions, their global total emission amounts differed by a factor of 3-4, ranging from 13.76 to 51.93 Tg for organic carbon and from 1.65 to 5.54 Tg for black carbon. In most regions, QFED2.4 and FEER1.0, which are based on the satellite observations of fire radiative power (FRP) and utilize the aerosol optical depth (AOD) from the Moderate Resolution Imaging Spectroradiometer (MODIS), yielded higher BB emissions than the rest by a factor of 2-4. In comparison, the BB emission from GFED4s and GFED3.1, which are based on satellite retrieval of burned area and no AOD constraints, were at the low end of the range. In order to examine the sensitivity of model simulated AOD to the different BB emission datasets, we ingested these six BB emission datasets separately into the same global model, the NASA Goddard Earth Observing System (GEOS) model, and compared the simulated AOD with observed AOD from the AErosol RObotic NETwork (AERONET) and MODIS in 14 sub-regions during 2008. In Southern hemisphere Africa (SHAF) and South America (SHSA), where aerosols tend to be clearly dominated by smoke in September, the simulated AOD were underestimated in all experiments. More specifically, the model-simulated AOD based on FEER1.0 and QFED2.4 were the closest to the corresponding AERONET data, being about 73% and 100% of the AERONET observed AOD at Alta-Floresta in SHSA, 49% and 46% at Mongu in SHAF, respectively. The simulated AOD based on the other four BB emission datasets accounted for only ~ 50% of the AERONET AOD at Alta Floresta and ~ 20% of at Mongu. Overall, during the biomass burning peak seasons, at most of the selected AERONET sites in each region, the AOD

https://doi.org/10.5194/acp-2019-475
Preprint. Discussion started: 8 July 2019

Atmospheric Chemistry and Physics Discussions

simulated with QFED2.4 were the highest and closest to AERONET and MODIS observations, followed closely by FEER1.0. The differences between these six BB emission datasets are attributable to the approaches and input data used to derive BB emissions, such as whether AOD from satellite observations is used as a constraint, whether the approaches to parameterize the fire activities are based on burned area, FRP, or active fire count, and which set of emission factors is chosen.

https://doi.org/10.5194/acp-2019-475
Preprint. Discussion started: 8 July 2019

Atmospheric Chemistry and Physics Discussions

1. Introduction

Biomass burning (BB) is estimated to contribute about 62% of the global particulate organic carbon (OC) and 27% of black carbon (BC) emissions annually (Wiedinmyer et al., 2011), thereby significantly affecting, not only air quality by acting as a major source of particulate matter (PM), but also the climate system by modulating solar radiation and cloud properties. For instance, a number of studies have revealed that wildfire smoke exposure is harmful to human health by causing general respiratory morbidity and exacerbating asthma, because approximately 80–90% of the smoke particles produced by biomass burning fall within the $PM_{2.5}$ size range (PM with aerodynamic diameter less than 2.5 μm) (Reid et al., 2005, 2016). Moreover, biomass burning emissions have been shown to impact the atmospheric composition in different regions, such as South America (Reddington et al., 2016), Central America (Wang et al., 2006), sub-Saharan African region (Yang et al., 2013), Southeast Asia (Wang et al., 2013; Pan et al., 2018), Indo-China (Zhu et al., 2017), and Western Arctic (Bian et al., 2013). Additionally, BB-produced aerosols can also directly impact the upper troposphere and lower stratosphere via extreme pyro-convection events associated with intense wildfires that generate the storms injecting smoke particles and trace gases into high altitudes (e.g., Peterson et al., 2018). Therefore, emissions from biomass burning constitute a significant component of the climate system, and are crucial inputs required by chemical transport and atmospheric circulation models used to simulate the atmospheric compositions, radiation, and circulation processes needed for air-quality and climate-impact studies (e.g., van Marle et al., 2017).

With the advent of satellite remote sensing of active fire and burned area products in the last couple of decades, a number of global BB emission datasets based on these observations have become available (e.g., Ichoku et al., 2012), for example, two BB datasets based on burned area approaches, namely, the Global Fire Emissions Database (GFED, van der Werf et al., 2006, 2010, 2017) and the Fire INventory from NCAR (FINN, Wiedinmyer et al., 2011), and three BB emissions datasets based on fire radiative power (FRP) approaches, namely, the Global Fire Assimilation System (GFAS, Kaiser et al., 2012), which was developed in the European Centre for Medium-Range Weather Forecasts (ECMWF), and two National Aeronautics and Space Administration (NASA) products, i.e., the Fire Energetics and Emissions Research algorithm (FEER, Ichoku and Ellison, 2014) and the Quick Fire Emissions Dataset (QFED, Darmenov and da Silva, 2015). The aforementioned BB datasets will be compared in this study.

Although much progress has been made over the last couple of decades in improving the quality of BB emission datasets, for example, by incorporating more recent satellite measurements with better calibration and spatial resolution (e.g., van der Werf et al. 2010; 2017), biomass-burning aerosol emissions still have large uncertainty, and thus are still poorly constrained in models at global and regional levels (e.g., Liousse et al., 2010; Kaiser et al., 2012; Petrenko et al., 2012, 2017; Bond et al., 2013; Zhang et al., 2014; Pan et al., 2015; Ichoku et al., 2016a; Reddington et al., 2016; Pereira et al., 2016). Specifically, large uncertainty exists in the description of the magnitude, patterns, and drivers of wildfires and other types of biomass burning (e.g., Hyer et al, 2011). For instance, a global enhancement of particulate matter BB emission by a factor of 3.4 was

https://doi.org/10.5194/acp-2019-475
Preprint. Discussion started: 8 July 2019

Atmospheric Chemistry and Physics
Discussions

recommended for GFAS by Kaiser et al. (2012) to match the observed aerosol loading. A recent analysis with multiple models has been conducted under the auspices of the Aerosol Comparisons between Observations and Models (AeroCom) Phase III biomass burning emission experiments using the GFED version 3.1 (GFED3.1) as input to several models (hereinafter, "multi-model study", https://wiki.met.no/aerocom/phase3-experiments) (Petrenko et al., manuscript in preparation). Multi-model study concluded that the modelled AOD from different models exhibits large diversity in most regions, i.e. some models overestimate while other models underestimate, but over two major biomass burning dominated regions, South America and southern hemisphere Africa, all models consistently underestimate AOD. That result suggests that the underestimation of AOD in these two regions is more likely from this biomass burning emission dataset (i.e., GFED3.1) rather than the model configurations.

Our study aims to explore multiple BB emission datasets, including GFED3.1, GFED version 4 with small fires (GFED4s), FINN version 1.5, GFAS version 1.2, QFED version 2.4, and FEER version 1.0, in order to investigate the discrepancies between these six BB emission datasets by comparing them at both regional and global levels. Such a comparative evaluation of BB emission datasets would show the differences between them as well how these differences propagate through the physical processes of related aerosols in models, such as dry and wet deposition, transport, atmospheric abundance, and the resulting AOD. The detailed diagnosis is expected to provide further insight into the development of possible mitigation measures for the current large uncertainties in BB emissions. It is noted that similar comparative studies of multiple BB aerosol emission datasets have been previously conducted at regional scales, e.g., by Zhang et al. (2014) in the northern sub-Saharan African region, Pereira et al. (2016) in South America, and Reddington et al. (2016) in entire tropical region, while the current study provides for the first time a global assessment and analysis of 14 sub-regions of these six BB emission datasets to provide a world-wide perspective.

In the rest of this paper, we first described these six BB emission datasets, the GEOS model configuration and experiment designs, and observations in Sect. 2, then we showed the comparison of biomass burning emissions among the datasets and the resulting model simulated AOD in Sect. 3. We discussed the possible attributions of the difference between the six BB emission datasets, and the sources of uncertainty associated with the biomass burning emissions as well as aerosol modeling in Sect. 4. Conclusions and recommendations were presented in Sect. 5.

2. Methodology

2.1 Six BB emission datasets

General information about each of the six biomass burning emission datasets investigated in this study, namely GFED3.1, GFED4s, FINN1.5, GFAS1.2, FEER1.0, and QFED2.4, is given below. Their main attributes, such as their spatial and temporal resolutions, the methods used to estimate burned area (where applicable), the method to derive emission coefficients (where applicable), and the references of the emission factors, are compared in Table 1. Overall, all datasets provide daily global biomass burning emissions since 2003.

https://doi.org/10.5194/acp-2019-475
Preprint. Discussion started: 8 July 2019

2.1.1 GFED3.1

The total dry matter consumed from biomass burning in GFED3.1 (van der Werf et al., 2010) is estimated by the multiplication of the MODIS burned area product at 500-m spatial resolution (Giglio et al. 2010, for the MODIS era) and fuel consumption per unit burned area, the latter being the product of the fuel loads per unit area and combustion completeness. This estimation is conducted using the Carnegie–Ames–Stanford approach (CASA) biogeochemical modeling framework that provides estimates of biomass in various carbon "pools" including leaves, grasses, stems, coarse woody debris, and litter. Fuel loads in CASA are estimated according to carbon input information on vegetation productivity, and carbon outputs through heterotrophic respiration, herbivory, fires, and tree mortality (Giglio et al., 2010; van der Werf et al., 2010; Randerson et al., 2012). Then, the biomass burning emission of a certain species is calculated by multiplying the total consumed dry matter with an emission factor of that species (*EF*, with a unit of g species per kg dry matter burned). *EF* is applicable to other BB emission datasets as well but may be from various sources, mainly chosen from Andreae and Merlet (2001) or Akagi et al. (2011). Among the existing BB emission datasets, GFED3.1 has hitherto been the most wildly used by modeling communities, such as by the Coupled Model Intercomparison Project (CMIP, Van Marle et al., 2017) and AeroCom (Petrenko 2017). The GFED3.1 dataset can be accessed through the link: https://daac.ornl.gov/VEGETATION/guides/global_fire_emissions_v3.1.html.

2.1.2 GFED4s

Compared to GFED3.1, the latest GFED version, GFED4s, has a few significant upgrades as described in detail by van der Werf et al. (2017), including (1) additional burned area associated with small fires which were previously omitted by the burned area product but now are compensated by including the active fires to augment the burned area product MCD64A1 (Giglio et al., 2013; Randerson et al., 2012); (2) a revised fuel consumption parameterization optimized using field observations (e.g., van Leeuwen et al., 2014); (3) partitioning of the extratropical forest category into temperate and boreal forests; (4) further dividing forest into temperate and boreal forest ecosystems and applying different sets of emission factors. The link to the GFED4s dataset is http://www.globalfiredata.org.

2.1.3 FINN1.5

The FINN1.5 biomass burning emission dataset is developed from its previous version FINN1 (Wiedinmyer et al., 2011) with several updates. It uses satellite observation of active fire (with confidence level greater than 20%) and land cover from the MODIS instruments onboard the NASA Terra and Aqua polar orbiting satellites, together with the estimated fuel consumption to derive biomass burning emissions. The burned area in each active fire pixel is assumed as 1 km^2, except for grasslands and savannas where it is assigned a value of 0.75 km^2. The fuel consumption at each fire pixel is estimated according to its generic land use/land cover type (LULC) which is assigned using values updated from Table 2 of Hoelzemann et al. (2004) in the various world regions based on Global Wildland Fire Emission Model (GWEM). With the estimated burned area, fuel consumption, and *EF* of individual species, the daily global open biomass burning

https://doi.org/10.5194/acp-2019-475
Preprint. Discussion started: 8 July 2019

emissions of each species are then calculated at a 1 km spatial resolution. The FINN1.5 emissions dataset is archived at: http://bai.acom.ucar.edu/Data/fire/.

2.1.4 GFAS1.2

GFAS1.2 (Kaiser et al., 2012) estimates biomass burning emission rates by multiplying FRP with the eight biome-specific conversion factors (Units: kg species per MJ) which were previously found to link FRP with the fuel combustion rate (Wooster et al., 2005) and smoke aerosol emission rate quantitatively (Ichoku and Kaufman, 2005). In GFAS, the global distribution of FRP observations obtained from the MODIS instruments onboard the Terra and Aqua satellites is assimilated into the GFAS system. The gaps in FRP observations, which are mostly due to cloud cover and spurious FRP observations of volcanoes, gas flares and other industrial activity, are corrected or filtered in the GFAS system (Kaiser et al., 2012). The eight biome-specific conversion factors are calculated by linear regressions between the GFAS FRP and the dry matter combustion rate of GFED3.1 in each biome (see Table 2 and Fig.3 in Kaiser et al.., 2012). Therefore, the biomass burning emission calculated by GFAS is close to that of GFED3.1. Then the biomass burning emission from a certain aerosol species is converted by multiplying the total consumed dry matter with *EF* of that species. More information on the latest GFAS product can be found at https://confluence.ecmwf.int/display/CKB/CAMS++Global+Fire+Assimilation+System+(GFAS)+data+documentation. The GFAS1.2 dataset can be downloaded at https://apps.ecmwf.int/datasets/data/cams-gfas/.

2.1.5 FEER1.0

The FEER1.0 (Ichoku and Ellison, 2014) uses FRP from the GFAS1.2 analysis system (Kaiser et al., 2012) multiplied by emission coefficient C_e (Units: kg species per MJ) to derive aerosol biomass burning emission rates; however, the way how C_e, which is called conversion factor by Kaiser et al. (2012), is derived in FEER1.0 is more sophisticated than that in GFAS1.2 (Kaiser et al., 2012). The C_e in FEER1.0 for smoke aerosol total particulate matter (TPM) is derived through zero-intercept regression of the emission rate of smoke aerosol (i.e., R_{sa}) against the corresponding FRP (Ichoku and Kaufman, 2005; Ichoku and Ellison, 2014) at pixel-level within each grid. C_e corresponds to the slope of the linear regression fitting. In the FEER methodology, R_{sa} is estimated through a spatio-temporal analysis of MODIS AOD data along with wind fields from the NASA Modern-Era Retrospective Analysis for Research and Applications (MERRA) reanalysis dataset (Rienecker et al., 2011). The smoke aerosol C_e in FEER1.0 is available at 1°×1° spatial resolution global grid, and covers most land areas where fires have been detected by MODIS for at least 30 times during the period 2003-2010 (Ichoku and Ellison, 2014) to ensure statistical representativeness. In the current version of FEER1.0 emission dataset, C_e for other smoke constituents, say OC, at each grid cell are obtained by scaling the C_e of smoke aerosol according to the ratio of their emission factors, such as EF_{oc} *to* EF_{sa} (i.e., ratio of emission factor for OC to that for total smoke aerosol). The FEER1.0 dataset is available at http://feer.gsfc.nasa.gov/data/emissions/.

2.1.6 QFED2.4

https://doi.org/10.5194/acp-2019-475
Preprint. Discussion started: 8 July 2019

The earlier version of QFED (Darmenov and da Silva 2015) estimated biomass burning emissions by multiplying level 2 MODIS FRP with an emission coefficient C_e which is the product of the initial constant value C_0 (1.37 kg per MJ, reported by Kaiser et al., 2009) and a scaling factor, with the scaling factor calculated by regressing the carbon monoxide (CO) BB emission (product of FRP, C_0 and CO emission factor) to that in the GFED version 2. The scaling factor used by the QFED 2.4, the version used in this study, was obtained by further regressing the Goddard Earth Observing System (GEOS) Model simulated AOD to the MODIS AOD in 46 sub-regions, and then the resulting scaling factors in the 46 sub-regions were aggregated into four major fire-prone biomes, i.e., savanna, grassland, tropical forests, and extratropical forests, as values of 1.8, 1.8, 2.5, and 4.5, respectively. The QFED2.4 also used a sequential model with temporally damped emissions to estimate the emissions in cloudy areas. The real-time QFED2.4 fire emission is produced on a daily basis and used in the operational GEOS data assimilation system. In addition to the near real-time emissions, a longer historical record dataset which we used is also maintained based on data from the MODIS Adaptive Processing System (MODAPS) Service (http://modaps.nascom.nasa.gov/services/).

2.2 Application of the BB emission datasets in the NASA GEOS model

2.2.1 Description of the NASA GEOS model

The GEOS model consists of an atmospheric general circulation model, a catchment-based land surface model, and an ocean model, all coupled together using the Earth System Modeling Framework (ESMF, Rienecker et al., 2011; Molod et al., 2015). Within the GEOS model architecture, several interactively coupled atmospheric constituent modules have been incorporated, including an aerosol and carbon monoxide (CO) module based on the Goddard Chemistry Aerosol Radiation and Transport model (GOCART, Chin et al., 2000, 2002, 2009, 2014; Colarco et al., 2010; Bian et al., 2010) and a radiation module from the Goddard radiative transfer model (Chou and Suarez, 1999; Chou et al., 2001). The GOCART module used in this study includes representations of dust, sea salt, sulfate, nitrate, and black and organic carbon aerosol species. A conversion factor of 1.4 is used to scale organic carbon mass to organic aerosol (OA), which is on the low end of current estimates (Simon and Bhave, 2012).

In this study the GEOS model (Heracles-5.2 version) was run globally on a cubed-sphere horizontal grid (c180, ~50 km resolution) and with 72 vertical hybrid-sigma levels extending from the surface to ~85 km for the year 2008. The model was run in a “replay” mode, where the winds, pressure, moisture, and temperature are constrained by the MERRA-2 reanalysis meteorological data (Gelaro et al., 2017), a configuration that allows a similar simulation of real events as in a traditional off-line chemistry transport model (CTM) but exercises the full model physics for, e.g., radiation, and moist physics processes. We used the HTAP2 anthropogenic emissions (Janssens-Maenhout et al., 2015) that provides high-spatial resolution monthly emissions. The BB emissions are uniformly distributed within the boundary layer without considering the specific injection height of each plume. All six BB emissions are daily emissions with the diurnal cycle prescribed in the model: the maximum is around local noon, which is more prominent in the tropics, gradually weakened in the extra-tropics (Randles et al., 2017). The natural

https://doi.org/10.5194/acp-2019-475
Preprint. Discussion started: 8 July 2019

aerosols are either generated by the model itself (i.e., wind-blown dust and sea salt) or from prescribed emission files (i.e., volcanic and biogenic aerosols).

2.2.2 Experiment design

In order to investigate the sensitivity of the modelled AOD to different BB emission datasets, seven experiments were conducted with the GEOS model, differing only in the source of biomass burning emissions. The first six runs are GFED3.1, GFED4s, FINN1.5, GFAS1.2, FEER1.0, and QFED2.4, using the corresponding biomass burning datasets described above in Section 2.1. A seventh run is called "NOBB," where the model is run without including biomass burning emissions.

2.4. AOD Observations

2.4.1 MODIS retrievals

We used the AOD retrieved from the MODIS collection 6 products from both the Terra and Aqua satellites with the combination of Dark Target (DT) aerosol algorithm (Remer et al., 2005; Levy et al., 2010), which was designed for aerosol retrievals over dark land (mostly vegetated) and ocean surfaces in the visible (VIS) to shortwave infrared (SWIR) parts of the spectrum, and the Deep Blue aerosol algorithm (Sayer et al., 2014), which was designed for aerosol retrieval over bright surfaces (e.g., desert).

2.4.2 AERONET sites

We also evaluated the modelled AOD at 550nm and Angstrom Exponent (AE, 440–870 nm) with that from the ground-based AErosol RObotic NETwork (AERONET, Holben et al., 1998) sites situated in biomass burning source regions. AERONET Version 3 Level 2.0 data, which are cloud-screened and quality-assured aerosol products with a 0.01 uncertainty (Giles et al., 2019), were used in this study. The AERONET AOD at 550nm is interpolated from the measurements at 440 and 675nm. Angstrom Exponent (AE) is calculated with AOD at 440 and 870nm. We compared model simulations with AERONET data at 14 selected sites, each representing the spatiotemporal characteristics at different biomass burning regions shown in Fig. 1 that are defined previously by the GFED studies (e.g., Van der Werf et al., 2006, 2010, and 2017). Some regions have no AERONET sites with data measured in 2008, i.e., Northern Hemisphere South America (NHSA) and Equatorial Asia (EQAS), we thus also showed the average of multiple years or climatology of AERONET AOD at each site for reference. Locations of these 14 selected AERONET sites are represented by the numbered magenta dots in Fig.1.

3. Results

3.1 Inter-comparison of the six biomass burning emission datasets

The OC biomass burning emissions were compared throughout this study, since OC is the major constituent in fresh biomass burning smoke particles, with mass fractions ranging from 37% to 67% depending on fuel type (e.g. grassland/savanna, forests, or others), according to various studies based on thermal evolution techniques (Reid et al., 2005, part II, Table 2). These inter-comparisons were carried out in terms of both annual and seasonal variations in Sect. 3.1.1 and Sect. 3.1.2 respectively.

3.1.1 Annual total

https://doi.org/10.5194/acp-2019-475
Preprint. Discussion started: 8 July 2019

Atmospheric Chemistry and Physics Discussions

Figure 2 shows the spatial distributions of annual total OC biomass burning emissions in 2008 from the six BB emission datasets. The hot spots in Africa, boreal Asia, and South America were pronounced in all six BB emission datasets, albeit to different degrees. The regional differences of the annual OC biomass burning emissions in different BB emission datasets can be appreciated more quantitatively in Fig. 3. Relevant statistics for the six BB emission datasets in the 14 regions were also listed in Fig. 3 at the top of the panel, with the annual mean averaged over the six BB emission datasets in the first row (*mean*). We used three different measures to quantify the spread of the six BB emission datasets: (1) standard deviation (*std*) of the annual mean, (2) ratio of maximum to minimum (*max/min*), and (3) the coefficient of variation (*cv*, defined as the ratio of the *std* to the *mean*). The rank of *cv* for each of the 14 regions was also listed in Fig. 3 (e.g., a ranking of 1 means that this region shows the least spread among the six BB emission datasets, while a ranking of 14 indicates that this region has the largest spread). The best agreements among the six emission datasets occurred in Northern Hemisphere Africa (NHAF), Equatorial Asia (EQAS), Southern Hemisphere Africa (SHAF), and Southern Hemisphere South America (SHSA), which have the top *cv* ranks (1-4) and relatively low *max/min* ratio (a factor of 3-4). The worst agreements occurred in Middle East (MIDE), Temperate North America (TENA), Boreal North America (BONA) and Europe (EURO), which have the bottom *cv* ranks (14-11) and large *max/min* ratio (a factor of 66-10). This diversity was mostly driven by the QFED2.4 emission dataset, which estimated the largest emission amount for almost all regions (except EQAS), especially in MIDE where BB emission from QFED2.4 is more than 50 times higher than that from other emission datasets. Globally, the QFED2.4 dataset showed the highest OC emission of 51.93 Tg C in 2008, which was nearly four times that of GFED4s of 13.76 Tg C (the lowest among the six BB datasets).

Overall, two FRP-based BB emissions, QFED2.4 and FEER1.0, were a factor of 2-4 larger than other BB datasets, which is consistent with the findings of Zhang et al. (2014) over sub-Saharan Africa. It is worth noting that the BB emission amount of GFAS1.2 was close to that of GFED3.1 confirming that GFAS1.2 is tuned to GFED3.1(described in Sect. 2.1.4). Globally, FINN1.5 yielded more OC emissions than the two GFED and GFAS1.2 datasets (e.g., 40% larger than the GFED4s). Regionally, FINN1.5 was generally comparable to the two GFED datasets in most regions, but was higher than them in the tropical regions, such as EQAS, Southeast Asia (SEAS), Central America (CEAM) and NHSA. Interestingly, the FINN1.5 was even the largest among all six datasets over EQAS region (i.e., the Tropical Asia), which might be associated with its assumption of continuation of burning into the second day over there (to be discussed in section 4.1.2). The global OC emissions from GFED4s were lower than those from its GFED3.1 counterpart, although higher in several regions, such as TENA, Central America (CEAM), Northern Hemisphere South America (NHSA), Boreal Asia (BOAS) and Central Asia (CEAS). Possible explanations for these differences among the six global BB emissions datasets are provided in Sect. 4.1.

3.1.2 Seasonal variation

Biomass burning is generally characterized by distinct seasonal variations in each of the 14 sub-regions and globally, as shown in Fig. 4. Overall, there were four peak fire

https://doi.org/10.5194/acp-2019-475
Preprint. Discussion started: 8 July 2019

seasons across the regions: (1) During the boreal spring (March-April-May), fires peak in BOAS mainly because of forest fires (see the contribution of different fire categories in Table 3 of van der Werf et al., 2017), in SEAS, CEAM, and NHSA because of savanna and deforestation fires, and in Central Asia (CEAS) mainly due to the agricultural waste burning to prepare the fields for spring crops. (2) During the boreal summer (June-July-August), fires peak in BONA and TENA, mostly due to wildfires that occur under the prevailing dry and hot weather, in EURO probably associated with the burning of agricultural waste, and in MIDE, although the seasonal maximum in QFED may have been significantly influenced by emissions from gas flares and other activities. (3) During the austral spring (September-October-November), fires peak in the southern hemispheric regions of SHSA, SHAF and AUST, associated with savanna burning (in addition to deforestation fires in SHSA); (4) During the boreal winter (December and January), fires peak in NHAF, particularly along the sub-Sahel belt (Fig. 2), where savanna fires are associated with agricultural management and pastoral practices across that region (e.g. Ichoku et al., 2016b). Overall, all six BB emission datasets exhibited similar seasonal variations, although they differed in magnitude. In particular, it is noteworthy that in EQAS, the annual OC emissions from GFED4s was lower than that of GFED3.1 by 18%, but higher in the month of April by a factor of two.

For reference, biomass burning black carbon (BC) emissions were also shown, but in the supplement (Fig. S1, S2 for annual mean and Fig. S3 for seasonal variation), which exhibited similar features as OC. The amounts of biomass burning BC emission were almost proportional to their OC counterparts (about 1/10 to 1/15 of OC).

3.2 Comparison of model-simulated AOD with remote sensing data

As in other similar situations where several different datasets are available to be chosen from (e.g. Bian et al., 2007), a question that invariably comes to mind is: which BB emission dataset is the most accurate or should be used in a given situation? In fact, it is difficult to give a conclusive answer, as it is often challenging to measure the emission rate of an active fire in real time or to disentangle the contribution of smoke aerosols from the total atmospheric aerosol loading/concentration in observations. Therefore, in this study we have implemented all six global BB emission datasets in the GEOS model, and evaluated the simulated aerosol loading associated with each BB emission dataset instead. More specifically, we compared the simulated AOD with the satellite-retrieved AOD data from MODIS (primarily to examine the spatial coverage) as well as with ground-based measurements from AERONET sites near biomass burning source regions to examine the seasonal variation. Our analysis was focused during biomass burning peak seasons, when smoke aerosol emissions dominate those from other sources, such as pollution or dust. With such an effort to evaluate the sensitivity of the simulated AOD to the different BB emission datasets, the results from this study may shed some lights on answering the aforementioned question, i.e., which BB dataset is the most accurate or should be used in a given situation? We acknowledge that although focusing on a particular model (e.g., GOES in this case) can potentially introduce additional uncertainty through various complicated and non-linear procedures employed to calculate the AOD, such as the modelled relative humidity and the related aerosol's hydroscopic growth (Bian et al., 2009; Pan et al., 2015), still, evaluation of the model-simulated AOD has proven to be a feasible approach to compare various BB emission datasets in reference to the currently available observations (e.g., Petrenko et al. 2012; Zhang et al., 2014).

Aiming to evaluate the sensitivity of the modelled AOD to different BB emissions datasets, we compared the spatial distribution of GEOS model-simulated AOD with MODIS-retrieved AOD in Sect. 3.2.1 and with the AERONET measured AOD at 14 AERONET sites in Sect. 3.2.2.

3.2.1 Global spatial distribution

Comparisons for September and April in 2018 are shown in Fig. 5 and Fig. 6 respectively, representing the peaking biomass burning months in the southern hemisphere and many regions in the northern hemisphere, respectively. The MODIS-Aqua AOD is displayed on the top left panel and the model biases relative to it (model minus MODIS) are shown on other panels in each of the two cases.

In September 2008, the high AOD observed from MODIS-Aqua (i.e., MODIS-a) in the Southern hemisphere (Fig. 5a) was mostly attributable to biomass burning. The observed AOD peaked in the region of SHAF with an area-averaged value as 0.351 (see the area-averaged value for each region in Table S1) and the adjacent eastern South Atlantic Ocean (>1.0), and gradually decreased westwards. The observed AOD was 0.199 averaged over SHSA with a maximum value of nearly 0.4 in western Brazil (Fig. 5a). Large negative biases of -0.301 and -0.140 in the regions of SHAF and SHSA respectively are found in the NOBB run (see Fig. 5b, Table S1 shows the area-averaged values). These negative biases were reduced to the largest degree in the QFED2.4 run, i.e., to -0.059 and 0.004 in these two regions respectively (See Fig. 5h), followed by the FEER1.0 run to -0.094 and -0.034 respectively (Fig. 5g). The reductions of negative biases were the least in GFED4s, only to -0.226 and -0.093 respectively (Fig. 5d), followed by GFAS1.2 (Fig. 5f).

In April 2008 (Fig. 6), biomass burring emissions peaked in the regions of Southeast Asia (SEAS), Central Asia (CEAS), Boreal Asia (BOAS), Central America (CEAM), and Northern Hemisphere South America (NHSA). FINN1.5 and QFED2.4 had the best agreement with MODIS-a in regions of SEAS and CEAM (see Table S1). Being mixed with, and often surpassed by other aerosol types, however, the contribution of biomass burning aerosols to the total AOD are hardly distinguishable in this month, especially if the simulated background AOD in NOBB (simulation without biomass burning emission) was already biased high relative to MODIS (e.g., in EURO-Europe). Such complicated situations occurred during most of other months (not shown), leading to the difficulties in evaluating the BB emission datasets with the AOD observations.

3.2.2 Seasonal variations of AOD at AERONET sites

In order to better quantify the sensitivity of the simulated AOD to the six different BB emission datasets, we further compared the simulated monthly AOD with the ground-based AOD observations from AERONET stations by choosing one representative station in each region (Fig. 7). The exception is in two regions NHSA and EQAS, where there are no valid AERONET observations during 2008, thus we used the multi-year climatology of AOD at Medellin and Palangkaraya to represent NHSA and EQAS, respectively. We also included the climatology of AERONET AOD in the other 12 AERONET sites for reference. As shown in Fig. 7, AOD in 2008 at available sites (brown thin bars) were similar to their respective climatology (light gray thick bars) within 0.05. The MODIS-t (Terra) and MODIS-a (Aqua) AOD were plotted for reference as purple diamond and blue triangle, respectively. In most cases, these two MODIS observations agreed with each other, with MODIS-Terra being the higher one at most sites except for Mongu and Lake_Argyle, where savanna burning is dominant. Note that the panels representing the AERONET stations in Fig. 7 were arranged in a way that their placements correspond to those of their respective regions in Fig. 4 for easy inter-comparison. In this section, the modelled monthly mean AOD was calculated by averaging over the modelled instantaneous AOD in each month; while the monthly AOD of AERONET and MODIS are simply calculated by averaging over available observations in each month.

In general, runs with different BB emission datasets showed almost identical AOD during non-biomass burning seasons in each region, thereby leaving their differences noticeable during the biomass burning peak seasons. The larger spread of the seven runs at each selected AERONET station usually occurred in the peak month(s) of biomass burning in respective region, as expected. At most other AERONET sites, the simulated AOD based on QFED2.4 were the highest and closest to AERONET AOD during the corresponding peak biomass burning seasons, followed by FEER1.0 and FINN1.5, and then GFED3.1, GFEDv4 and GFAS1.2. Meanwhile, contributions from non-BB emissions to the total AOD are represented by NOBB experiment (black line in Fig. 7). The contribution of non-BB AOD was more than that of BB AOD during the burning seasons at most selected AERONET sites, except at Alta Floresta (Fig. 7.5), Mongu (Fig. 7.9), and Chiang Mai Met Sta (Fig. 7.12). Model simulations had difficulty representing the non-BB AOD at three high-latitude (> 55°N) AERONET sites almost year around, i.e., Fort McMurray in BONA, Toravere in EURO, and Moscow_MSU_MO in BOAS (three panels in the top row of Fig. 7). However, the simulated AOD with QFED2.4 were apparently overestimated during October and November at Fort McMurray.

3.3 Case studies in biomass burning dominated regions

In order to investigate the relationship between AOD and biomass burning emission, we focused on two AERONET stations, namely, Alta Floresta in SHSA and Mongu in SHAF, for the in-depth analysis in this section in the context of daily variation during September. Biomass burning emissions are known to be dominant at such locations and month as estimated by Chin et al. (2009). They found that 50-90% of the AOD was attributable to biomass burning emissions using a GOCART model simulation. Based on previous studies, e.g., Pereira et al. (2016) in SHSA, and Reddington et al. (2016) in tropical regions including SHSA and SHAF, there appears to be a general consensus that the simulated AOD is consistently underestimated over these two regions in many models with different BB emission datasets. We calculated the 3-hourly AOD by sorting the instantaneous AOD from both AERONET and model outputs on each day into eight time-steps, namely, 0, 3, 6, 9, 12, 15, 18, and 21Z. In this section, the modelled monthly mean AOD was calculated by averaging over the modelled 3-hourly AOD, which

https://doi.org/10.5194/acp-2019-475
Preprint. Discussion started: 8 July 2019

Atmospheric Chemistry and Physics
Discussions

coincided with 3-hourly AERONET AOD in that month. The detailed analyses are discussed below.

3.3.1 Alta Floresta in South America

The monthly averaged AOD observed from AERONET at Alta Floresta is 0.47 during September 2008 (Fig. 8a). Figure 8a shows that the simulated AOD from all six experiments captured the sustained aerosol episode observed in the AERONET dataset in the middle of September, on September 13-14 (AOD about 1.0-1.5). The simulation with QFED2.4 BB emission produced the closest agreement with the AERONET-observed AOD with an average *ratio* of 1.00. In contrast, the simulated AOD with FEER1.0, FINN1.5, GFAS1.2, GFED3.1, and GFED4s emissions tended to underestimate most of the time, with GFED4s having the largest negative bias (*ratio*=0.36). The AE (an indicator of particle size) from AERONET is 1.66 (not shown), indicating that smoke particles are from burning of both forests and grasses at Alta Floresta (Eck et al., 2001). All experiments matched the observed AE (now shown).

There was a large contrast of local biomass burning OC emission between September 24-25 (as high as 1-2 μg m^{-2} s^{-1}) and the other days (close to zero) (Fig. 8b). Such sharp contrast was completely missing in the simulated AOD (Fig. 8a). Nevertheless, the OC column dry mass load (Fig. 8c) resembled with the corresponding AOD (Fig. 8a), implying that the day-to-day variation of relative humidity (RH) in the dry season is too small to influence the AOD. All experiments showed relatively low skill of capturing the temporal variability of the observed AOD at Alta Floresta (*corr*=0.24-0.60). All these evidences, therefore, collectively suggest that the temporal variations of AOD (and aerosol mass loading) in Alta Floresta during the burning season do not directly respond to the local BB emission at the daily and sub-daily time scales. Other processes which determine the residence time of aerosols (typically a few days), such as the regional scale transport and removal, likely play critical roles in determining the local aerosol loading. The MODIS-Terra true color image overlaid with fire hotspots (red dots) on September 13, 2008 confirms that dense smoke over Alta Floresta (blue circle) was transported from the upwind areas instead from local BB emissions during this peak aerosol episode (Fig. 8d). Thus, accurate estimation of regional emissions and representations of regional scale transport and removal are rather important.

3.3.2 Mongu in Southern Hemisphere Africa

The case at Mongu is different from that of Alta Floresta. There were numerous fire hot spots (represented by the red dots in this MODIS-Aqua true color image) at and close to Mongu (blue circle), as revealed by Fig. 9d on September 12, 2008, one of peak aerosol episodes. The visibility over entire region was apparently low due to smoke aerosols. Accordingly, the biomass burning OC emissions averaged over the grid box of Mongu exhibited distinct daily variations in each BB dataset (Fig. 9b). Similar emission patterns are found when averaged over nine or 25 surrounding grid boxes (not shown). At this site, the day-to-day variations of AOD still cannot be totally explained by the corresponding emission at Mongu. For example, emission from FEER1.0 on September 17 is six times higher than that on September 2 (Fig. 9b) but the simulated AOD on September 17 is twice lower than that on September 2 (Fig. 9a). Although the temporal

https://doi.org/10.5194/acp-2019-475
Preprint. Discussion started: 8 July 2019

Atmospheric Chemistry and Physics
Discussions

variation of the ambient RH may partially contribute to the day-to-day changes of the emission-AOD relationship, the close resemblance between the model simulated AOD and column OC dry mass loading (Fig. 9c) excludes such possibility. All model experiments almost reproduced the AERONET AE throughout September at this site (not shown), which is 1.80, confirming the dominance of the fine-mode aerosol particles emitted from smoke aerosols that is captured by the model irrespective of the BB emission dataset used. These evidences therefore suggest again that the temporal variations of AOD (and aerosol mass loading) in Mongu, where local emissions were present, do not also directly respond to the local BB emission at the daily and sub-daily time scales during the burning season, further confirming the importance of accurate estimation of regional emissions and representations of regional scale transport and removal as aforementioned in the case of Alta Floresta.

On broader spatial scales, AOD at Mongu did closely vary with the BB emission. It is apparent that overall higher BB emissions still resulted in higher column mass loading and thus AOD in general, as indicated by comparing six BB emission datasets. For instance, FEER1.0 and QFED2.4, which had the largest month total biomass burning OC emission among the six BB emission datasets during September over the region of SHAF (2.27 and 2.92 Tg mon^{-1} respectively in Fig. 4), resulted in the highest AOD (*ratio*=49% and 46% of the observed respectively in Fig. 9a); while FINN1.5 and GFED4s, which represented the lowest monthly mean biomass burning OC emission among the six BB emission datasets (0.87 and 0.85 Tg mon^{-1} respectively in Fig.4), resulted in very low AOD (15% and 19% of the observed respectively).

Considering regional scale transport and removal processes as well as wind fields are the same across six BB emission experiments since they were run under the same model configurations, therefore, enhancement of BB emission amounts in all BB emission datasets (although in different degrees) in the region of Mongu are suggested by this study based on the results of AOD. The similar suggestion is applicable to the region of Alta Floresta (except for QFED2.4).

4. Discussion

The simulated AOD is biased low in biomass burning dominated regions and seasons as demonstrated in this study. More explanations on differences among the six BB emissions datasets are discussed in Sect. 4.1. Basically, the uncertainty of the simulated AOD could be attributable to two main sources: (1) BB emissions-related biases, (2) Model-related biases, which are discussed in Sections 4.2 and 4.3, respectively.

4.1 The possible explanations of differences among the six BB emission datasets

4.1.1 Higher BB emissions estimated from QFED2.4 and FEER1.0

This study has shown that the QFED2.4 and FEER1.0 BB emission datasets are consistently higher than the others, with QFED2.4 being the highest overall. Some of the possible reasons responsible for this difference includes:

Constrains with MODIS AOD. The emission coefficients (C_e) used to derive biomass burning emissions in both QFED2.4 and FEER1.0 are constrained by the MODIS AOD, although in different ways (detailed in Sec.2.1.6 and 2.1.5 respectively). This is not the case for other BB emission datasets especially GFAS1.2 which also uses the same FRP products in deriving dry mass combustion rate as FEER1.0 but tuned to the GFED3.1 dry matter combustion rate instead. QFED2.4 applied four biome-dependent scaling factors to the initial constant value C_0 when deriving its C_e, by minimizing the discrepancy between the AOD simulated by the GEOS model and the MODIS AOD in the respective biomes. The resulting scaling factors are 1.8 for savanna and grassland fires, 2.5 for tropical forests, and 4.5 for extratropical forests (Darmenov and da Silva 2015). This partially explains its very high emission over the extratropical regions of TENA, BONA and BOAS relative to the other emission datasets (Fig. 2-4). However, the high BB emission estimated by QFED2.4 is questionable during October and November of 2008 in the region of BONA (Fig. 4) according to the evaluation of its resulting AOD relative to the AERONET AOD at the site Fort McMurray (Fig. 7.1). As for FEER1.0, the process of deriving C_e involved calculating the near-source smoke-aerosol column mass with the MODIS AOD (total minus the background) for individual plumes, thereby limiting influence from other emission sources (Ichoku and Ellison, 2014).

Fuel consumption. In general, the FRP-based estimation such as QFED2.4 and FEER1.0 may enable more direct estimates of fuel consumption from energy released from fires, without being affected by the uncertainties associated with the estimates of fuel loads and combustion completeness (e.g., Kaufman et al., 1998; Wooster et al., 2003, 2005; Ichoku and Kaufman, 2005; Ichoku et al., 2008). However, FRP from non-BB sources, such as the gas flare, could be mistakenly identified as BB sources (one example is the possible misidentification of fires in MIDE by QFED2.4) thus requiring additional screening.

4.1.2 Features of FINN1.5

Globally, the FINN1.5 dataset is lower than QFED2.4 and FEER1.0, but larger than GFAS1.2, GFED3.1 and GFED4s (Fig. 3). Although FINN1.5 can capture the location of the large wildfires using the active fire products, the estimation of burned area is rather simple without the complicated spatial and temporal variability in the amount of burned area per active fire detection or variability in fuel consumption within biomes. For example, it estimates 1 km^2 burned area per fire pixel for all biomass types except for savanna and grassland where 0.75 km^2/fire pixel is estimated instead. That might partially explain why the FINN1.5 is extremely low in AUST, as suggested by Wiedinmyer et al. (2011). Additionally, the FINN1.5 dataset is the least over boreal regions, such as in regions of BOAS and BONA, where the FINN1.5 is only 1/3 and 3/5 of the GFED4s respectively. Large forest fires dominate in BOAS and BONA, so that the direct mapping of burned area as done in the GFED4s and GFED3.1 has more biomass burning emissions (van der Werf et al., 2017). On the other hand, the BB emission in FINN1.5 dataset is relatively large near the equator. For instance, it is the largest among the six datasets over the region EQAS, and the second largest over the regions of CEAM and SEAS. This might be attributed to the smoothing of the fire detections in these tropical regions to compensate for the lack of daily coverage by the MODIS instruments (Wiedinmyer et al., 2011): for each fire detected in the equatorial region only, a fire is counted for a 2-day period in FINN1.5, by assuming that fire continues into the next day but at half of its original size.

https://doi.org/10.5194/acp-2019-475
Preprint. Discussion started: 8 July 2019

Atmospheric Chemistry and Physics Discussions

4.1.3 Difference between GFED4s and GFED3.1

Globally and in some regions, OC biomass burning emission in GFED4s is lower than that in GFED3.1 (see Fig. 2-4), although the former has 11% higher global carbon emissions and includes small fires. There are a few possible reasons: 1) For aerosols, the implementation of lower *EF* for certain biomes in GFED4s than in GFED3.1 reduces the aerosol biomass burning emissions. As for the savanna and grassland, for instance, the GFED4s dataset mainly applies *EF* values recommended by Akagi et al. (2011), which are 2.62 g OC per kg dry matter burned, 18% lower than *EF* from Andreae and Merlet (2001) used in GFED3.1 (see Table 2); 2) In addition, the improvement on inclusion of small fires in GFED4s over GFED3.1 is offset by the occasional optimization of fuel consumption using field observations for overall carbon emissions. For instance, the turnover rates of herbaceous leaf (e.g., savanna) are increased in GFED4s, leading to the lower fuel loading and thus lower consumption for this land-cover type in GFED4s (van Leeuwen et al., 2014; van der Werf et al., 2017). Therefore, the OC biomass burning emissions are lower in GFED4s over SHAF, NHAF, and AUST (Fig. 3 and 4), where ~88% of carbon emission is from savanna and grassland (van der Werf et al., 2017).

On the other hand, there are regions in the northern hemisphere where GFED4s is higher than GFED3.1, for example, over CEAS and EURO, where small fires associated with burning of agricultural residues contribute to 43.6% and 58.6% of the carbon emissions (van der Werf et al., 2017). In spite of the 30% reduction of the *EF* in these two regions, the effect of including small fires in GFED4s exceeds, resulting in twice as high OC biomass burning emission from GFED4s as that from GFED3.1. Another example is in BOAS where the OC biomass burning emissions is 10% higher in GFED4s than in GFED3.1. It is likely attributable to a higher *EF* used in the former BB dataset than in the latter one for boreal forest fire in BOAS (9.60 vs. 9.14 g OC per kg dry matter, see Table 2), where 86.5 % of the carbon emission is from the Siberian forest (van der Werf et al., 2017).

It is interesting that the yearly total biomass burning OC emission from GFED4s is 20% lower than that from GFED3.1 in EQAS (Fig. 4), even though the small fires are included and the *EF* of peatland and tropical forest are higher in the former (Table 2). By examining the monthly variations over EQAS (Fig. 4), however, we found that GFED4s is actually higher than GFED3.1 in August by a factor of two when peatland burning is predominant, but equal to or lower than GFED3.1 in other months, particularly in May, leading to the overall lower annual total value in GFED4s.

4.2 Sources of the uncertainty associated with biomass burning emissions

Uncertainty in any of the six BB emissions datasets considered in this study could have been introduced from a variety of measurement and/or analysis procedures, including: detection of fire hot spots or area burned, retrieval of FRP, emission factors (see Table 1), land cover maps, and fuel consumption estimates, some of which are explained in detail below.

Fire detection. Most of the current global estimation of biomass burning emissions are heavily dependent on polar-orbiting satellite measurements from MODIS on Terra and

Aqua (e.g., MCD14DL, MOD14A1, MYD14A1, and MCD14ML as listed in Table 1). The temporal and spatial resolutions of these measurements impose limitations on their ability to detect and characterize the relevant attributes of fires, such as the locations and timing of active fires and the extent of the burned areas. Each of the two MODIS sensors, from which all of the major BB datasets derive their inputs, can only possibly observe a given fire location twice in 24 hours, which leaves excessive sampling gaps in the diurnal cycle of fire activity. Even for these few times that MODIS makes observations at its nominal spatial resolution of 1 km at nadir, it has the potential to miss a significant number of smaller fires (e.g. Hawbaker et al., 2008, Burling et al, 2011, Yokelson et al., 2011), as well as to miss fires obstructed by clouds and those located in the gaps between MODIS swaths in the tropics (Hyer et al., 2009; Wang et al., 2018). These issues can propagate into the uncertainties of the emissions datasets that are dependent on active fire detection product, especially those based on FRP, e.g., GFAS1.2 (Kaiser et al., 2012), FEER1.0 (Ichoku and Ellison, 2014), QFED2.4 (Darmenov and da Silva, 2015), as well as FINN1.5 (Wiedinmyer et al., 2011) which does not use FRP product but uses active fire product to derive burned area, and even GFED4s which does not use FRP either but uses active fire product to derive burned area for small fires.

On the other hand, although the sparse diurnal sampling frequency may not necessarily be an issue for the MODIS burned area product, upon which some of the emission datasets are based (*e.g.*, GFED3.1), burned area product may not account for small fires due to its low spatial resolution of 500-m, which may limit the identification of small burned scares such as those generated by small fires from crop lands (fire size < 21 ha). In addition, MODIS fire detection sensitivity is reduced at MODIS off nadir views, with increasing view zenith angles especially toward the edge of scan, where its ground pixel size is almost a factor of 10 larger (Peterson and Wang, 2013; Roberts et al., 2009; Wang et al., 2018), resulting in dramatic decreases in the total number of detected fire pixels and total FRP (Ichoku et al., 2016b; Wang et al., 2018). Moreover, all operational remote sensing fire products have difficulty accounting for understory fires or fires with low thermal signal or peatland fires such as those in Indonesia, where smoldering can last for months (Tansey et al, 2008).

Emission factor (EF). The *EF*, used for deriving individual particulate or gaseous species of smoke emissions from burned dry matter in all major BB emission datasets, heavily depends on the literature compiled by Andreae and Merlet (2001) and Akagi et al. (2011). The *EF* can have significant uncertainties. In general, most *EF*s are derived from very few lab-based studies whereby samples of fuels are burned in combustion chambers (i.e. Christian et al., 2003; Freeborn et al., 2008), where the combustion characteristics can be very different from those of large-scale open biomass burning and wildfires. It is somewhat surprising that the aerosol emissions from GFED4s are lower than those from GFED3.1 in most savanna regions (e.g., SHAF), even though the former includes smaller fires and has 11% higher global carbon emissions. This discrepancy between GFED4s and GFED3.1 can be partially explained by the fact that different emission factors were used to derive these two products, as explained earlier in Sect. 4.1.3.

https://doi.org/10.5194/acp-2019-475
Preprint. Discussion started: 8 July 2019

Burning stages. Furthermore, most current BB emission datasets do not distinguish the different burning stages, such as the flaming and smoldering stages that have distinctive emission characteristics. Typically, flaming dominates the earlier stage of the fire while smoldering dominates the later part. In the case of boreal forest fires, for example, about 40% of combustion originates from the flaming phase while 60% comes from the smoldering phase (Reid et al., 2005). In addition, smoldering combustion produces more OC and CO than flaming combustion; whereas flaming combustion produces more BC and carbon dioxide (CO_2) than smoldering (e.g., Freeborn et al., 2008).

4.3 Sources of the uncertainty associated with aerosol modeling

The model-related biases in the GEOS model, which other models most probably also suffer from, include, for example, inaccurate representations of horizontal and vertical transport of aerosol with wind, fire emission plume height, estimation of aerosol removal in models, and other model assumptions. Modeling of AOD properties such as optical properties and water uptake probably generates additional uncertainty. The ratio of OA to OC is 1.4 in this study, which is at the low end of the generally suggested range of 1.4-2.3. Observations suggest that OA/OC values of 1.6± 0.2 should be used for urban aerosols and 2.1± 0.2 for non-urban aerosols respectively (Turpin and Lim, 2001; Aiken et al., 2008). Enhancing this ratio can obviously increase the resulting AOD, but a more accurate measurement of this ratio during biomass burning is needed. Furthermore, the production of secondary organic aerosol (SOA) in biomass burning plumes, which has been observed in lab studies and ambient plumes (e.g., Bian et al., 2017; Ahern et al., 2019), are missing in these GEOS simulations. In addition, Ge et al. (2017) have shown that the choice of different meteorological fields, such as those from ECMWF and National Centers for Environmental Prediction (NCEP), can yield a factor of two difference in the resulting surface $PM_{2.5}$ concentration during the fire season of September in the Maritime continents.

5. Conclusions and recommendations

In this study, we compared six global biomass burning aerosol emission datasets in 2008, i.e., GFED3.1, GFED4s, FINN1.5, and GFAS1.2, FEER1.0 and QFED2.4. We also have examined the sensitivity of the modelled AOD to the different BB emission datasets in the NASA GEOS model globally and in 14-subregions. The main results are summarized as follows:

a. The biomass burning emissions derived from GFED3.1, GFED4s, FINN1.5, GFAS1.2, FEER1.0, and QFED2.4 can differ by up to a factor of 3.8 for OC on annual average, with values of 15.65, 13.76, 19.48, 18.22, 28.48, and 51.93 Tg C in 2008, respectively. In general, higher emissions are estimated from QFED2.4 globally and regionally, followed by FEER1.0.
b. The best agreement among the six emission datasets occurred in Northern Hemisphere Africa (NHAF), Equatorial Asia (EQAS), Southern Hemisphere Africa (SHAF), and South Hemisphere South America (SHSA), where the biomass burning emissions are predominant in determining aerosol loading, with the top coefficient of variation ranks (1-4) and relatively low *max/min* ratio (a factor of 3-4); and the least agreement occurred in Middle East (MIDE), Temperate North America (TENA), Boreal North America (BONA) and Europe (EURO) with the bottom coefficient of

variation ranks (14-11) and large *max/min* ratio (a factor of 66-10), where the biomass burning is either not dominant in total aerosol loading or QFED2.4 is extremely large. It seems that the diversity among the six BB emission datasets is largely driven by QFED2.4, which estimates the largest emission amount for almost all regions (except for equatorial Asia).

c. In SHAF and SHSA during September 2008, where and when biomass burning aerosols are dominant over other aerosol types, the amounts of OC biomass burning emissions from QFED2.4 and FEER1.0 are at least double those from the remaining BB emission datasets. The AOD simulated by the NASA GEOS based on these two BB emission datasets are the closest to those from MODIS and AERONET, but still biased low. In particular, at Alta Floresta in SHSA, they can account for 36%-100% of the observed AOD, and at Mongu in SHAF, the simulated AOD with six biomass burning emission datasets only account for 15%-49% of the observed AOD. Overall, during the biomass burning peak seasons at most representative AERONET sites selected in each region, the AOD simulated by QFED2.4 is the highest and closest to AERONET and MODIS observations, followed by FEER1.0. Considering regional scale transport and removal processes as well as wind fields are the same across six BB emission experiments since they were run under the same model configurations, therefore, enhancement of BB emission amounts in all BB emission datasets (although in different degrees) in the regions of Mongu and Alta Floresta are suggested by this study based on the results of AOD. We acknowledge that the result of this study is partially model-dependent, nevertheless, it sheds some light on our understanding of the uncertainty of the simulated AOD associated with the choice of aerosol biomass burning emission datasets.

Based on the results from the current study, it is appropriate to make some recommendations for future studies on improving BB emission estimation. Our understanding of the complexity, variability, and interrelationships between different fire characteristics (behavior, energetics, emissions) need to be improved (Hyer et al, 2011). For example, more accurate estimation of emission factors (*EF*) for different ecosystem types and burning stages would greatly improve the emission overall, as demonstrated by the discrepancy between GFED3.1 and GFED4s (see Sect. 4.1.3). The evaluation in this study is solely based on remote sensing AOD data. More global dense and continuous surface measurements are needed to validate the fire-generated aerosol loading in specific contexts, including surface and vertical aerosol concentrations and aerosol compositions, especially in the major BB regions.

Author contribution

CI, MC, and XP conceived this project. XP conducted the data analysis and the model experiments. XP and CI wrote the majority of this manuscript, and all other authors participated in the writing process and interpretation of the results. HB, AD, PC and AS helped on model set-up. CI, AD, and LE provided the biomass burning emission datasets and interpretation of these datasets. TK, JW, and GC provided the help to apply the biomass burning emission datasets in the model. CI and MC provided funding supports.

Acknowledgement

We thank the Goddard Earth Science Data and Information Services Center for providing gridded satellite products of MODIS through their Giovanni website. We thank the AERONET networks for making their data available. Site PIs and data managers of those networks are gratefully acknowledged. We acknowledge the use of imagery from the NASA Worldview application (https://worldview.earthdata.nasa.gov), part of the NASA Earth Observing System Data and Information System (EOSDIS). Computing resources supporting this work were provided by the NASA High-End Computing (HEC) Program through the NASA Center for Climate Simulation (NCCS) at Goddard Space Flight Center. We also thank the providers of biomass burning emission datasets of GFED, FINN, and GFAS. We acknowledge supports from various NASA earth science programs, including the NASA Atmospheric Composition Modeling, Analysis, and Prediction Program (ACMAP), the Modeling, Analysis, and Prediction program (MAP), and the Interdisciplinary Studies Program (IDS). XP also acknowledges the discussion with Dr. Dongchul Kim.

Reference

Ahern, A. T., Robinson, E. S., Tkacik, D. S., Saleh, R., Hatch, L. E., Barsanti, K. C., et al. Production of secondary organic aerosol during aging of biomass burning smoke from fresh fuels and its relationship to VOC precursors. Journal of Geophysical Research: Atmospheres,124. https://doi.org/10.1029/2018JD029068, 2019.

Aiken, A. C., Decarlo, P. F., Kroll, J. H., Worsnop, D. R., Huffman, J. A., Docherty, K. S., Ulbrich, I. M., Mohr, C., Kimmel, J. R., Sueper, D., Sun, Y., Zhang, Q., Trimborn, A., Northway, M., Ziemann, P. J., Canagaratna, M. R., Onasch, T. B., Alfarra, M. R., Prevot, A. S. H., Dommen, J., Duplissy, J., Metzger, A., Baltensperger, U., and Jimenez, J. L.: O/C and OM/OC ratios of primary, secondary, and ambient organic aerosols with highresolution time-of-flight aerosol mass spectrometry, Environ. Sci. Technol., 42, 4478–4485, doi:10.1021/es703009q, 2008.

Akagi, S. K., Yokelson, R. J., Wiedinmyer, C., Alvarado, M. J., Reid, J. S., Karl, T., Crounse, J. D., and Wennberg, P. O.: Emission factors for open and domestic biomass burning for use in atmospheric models, Atmos. Chem. Phys., 11, 4039–4072, https://doi.org/10.5194/acp-11-4039-2011, 2011.

Andreae, M. O. and Merlet, P.: Emission of trace gases and aerosols from biomass burning, Global Biogeochem. Cy., 15, 955–966, https://doi.org/10.1029/2000GB001382, 2001.

Bian, H., M. Chin, R. Kawa, B. Duncan, A. Arellano Jr., and R. Kasibhatla, Uncertainty of global CO simulations constraint by biomass burning emissions. J. Geophys. Res., 112, D23308, doi:10.1029/2006JD008376, 2007.

Bian, H., Chin, M., Rodriguez, J. M., Yu, H., Penner, J. E., and Strahan, S.: Sensitivity of aerosol optical thickness and aerosol direct radiative effect to relative humidity, Atmos. Chem. Phys., 9, 2375-2386, https://doi.org/10.5194/acp-9-2375-2009, 2009.

Bian, H., M. Chin, S. R. Kawa, H. Yu, T. Diehl, Multi-scale carbon monoxide and aerosol correlations from MOPITT and MODIS satellite measurements and GOCART

https://doi.org/10.5194/acp-2019-475
Preprint. Discussion started: 8 July 2019

model: implication for their emissions and atmospheric evolutions, J. Geophys. Res., 115, D07302, doi:10.1029/2009JD012781, 2010.

Bian, H., P. Colarco, M. Chin, G. Chen, J.M. Rodriguez, Q. Liang, et al. Investigation of source attributions of pollution to the Western Arctic during the NASA ARCTAS field campaign. Atmos. Chem. and Phys., 13, 4707-4721, doi:10.5194/acp-13-4707-2013, 2013.

Bian, Q., Jathar, S. H., Kodros, J. K., Barsanti, K. C., Hatch, L. E., May, A. A., Kreidenweis, S. M., and Pierce, J. R.: Secondary organic aerosol formation in biomass-burning plumes: theoretical analysis of lab studies and ambient plumes, Atmos. Chem. Phys., 17, 5459-5475, https://doi.org/10.5194/acp-17-5459-2017, 2017.

Bond, T., Doherty, S. J., Fahey, D. W., Forster, P. M., Berntsen, T., DeAngelo, B. J., Flanner, M. Ghan, Kärcher, B., Koch, D., Kinne, S., Kondo, Y., Quinn, P. Sarofim, M. C., Schultz, M., Schulz, M., Venkataraman, C., Zhang, H., Zhang, S., Bellouin, N. Guttikunda, S. Hopke, P. K., Jacobson, M. Z., Kaiser, J. W., Klimont, Z., Lohmann, U., Schwarz, J. P., Shindell, D., Storelvmo, T., Warren, S. G., and Zender, C. S.: Bounding the role of black carbon in the climate system: A scientific assessment, J. Geophys. Res., 118, 5380–5552, doi:10.1002/jgrd.50171, 2013.

Buchard, V., C. A. Randles, A. da Silva, A. S. Darmenov, et al.The MERRA-2 Aerosol Reanalysis,1980-onward, Part II: Evaluation and Case Studies. Journal of Climate, doi:10.1175/jclid-16-0613.1, 2017.

Burling, I. R., Yokelson, R. J., Akagi, S. K., Urbanski, S. P., Wold, C. E., Griffith, D. W. T., Johnson, T. J., Reardon, J., and Weise, D. R.: Airborne and ground-based measurements of the trace gases and particles emitted by prescribed fires in the United States, Atmos. Chem. Phys. Discuss., 11, 18677–18727, doi:10.5194/acpd-11-18677-2011, 2011.

Chin, M., R. B. Rood, S.-J. Lin, J.-F. Müller, and A. M. Thompson, Atmospheric sulfur cycle in the global mdel GOCART: Model description and global properties, J. Geophys. Res., 105, 24,661-24,687, 2000.

Chin, M., P. Ginoux, S. Kinne, O. Torres, B. N. Holben, B. N. Duncan, R. V. Martin, J. A. Logan, A. Higurashi, and T. Nakajima, Tropospheric aerosol optical thickness from the GOCART model and comparisons with satellite and sun photometer measurements, J. Atmos., Sci., 59, 461-483, 2002.

Chin, M., T. Diehl, O. Dubovik, T. F. Eck, B. N. Holben, A. Sinyuk, and D. G. Streets, Light absorption by pollution, dust and biomass burning aerosols: A global model study and evaluation with AERONET data, Ann. Geophys., 27, 3439-3464, 2009.

Chin, M., T. Diehl, Q. Tan, J. M. Prospero, R. A. Kahn, L. A. Remer, H. Yu, A. M. Sayer, H. Bian, I. V. Geogdzhayev, B. N. Holben, S. G. Howell, B. J. Huebert, N. C. Hsu, D. Kim, T. L. Kucsera, R. C. Levy, M. I. Mishchenko, X. Pan, P. K. Quinn, G. L.

Atmospheric Chemistry and Physics
Discussions

Schuster, D. G. Streets, S. A. Strode, O. Torres, and X.-P. Zhao, Multi-decadal variations of atmospheric aerosols from 1980 to 2009: a perspective from observations and a global model, Atmos. Chem. Phys., 14, 3657-3690, 2014.

Chou, M.-D. and M. J. Suarez, A solar radiation parameterization for atmospheric studies, NASA/TM-1999- 104606, Vol. 15, 1999.

Chou, M.-D., M. J. Suarez, X.-Z. Liang, and M.-H. Yan, A thermal infrared radiation parameterization for atmospheric studies. NASA Tech. Memo. 104 606, 55 pp, 2001.

Christian, T., Kleiss, B., Yokelson, R. J., Holzinger, R., Crutzen, P. J., Hao, W. M., Saharjo, B. H., and Ward, D. E.: Comprehensive laboratory measurements of biomass-burning emissions: 1. Emissions from Indonesian, African, and other fuels, J. Geophys. Res., 108(D23), 4719, doi:10.1029/2003JD003704, 2003.

Colarco, P. R., A. da Silva, M. Chin, T. Diehl. Online simulations of global aerosol distributions in the NASA GEOS-4 model and comparisons to satellite and ground-based aerosol optical depth, J. Geophys. Res., 115, D14207, doi:10.1029/2009JD012820, 2010.

Darmenov, A. and da Silva. A. The quick fire emissions dataset (QFED)–documentation of versions 2.1, 2.2 and 2.4, NASA Technical Report Series on Global Modeling and Data Assimilation, NASA TM-2015-104606, 38, 2015.

Eck, T. F., Holben, B. N., Ward, D. E., Dubovik, O., Reid, J. S., Smirnov, A., et al.. Characterization of the optical properties of biomass burning aerosols in Zambia during the 1997 ZIBBEE field campaign. Journal of Geophysical Research, 106(D4), 3425–3448. https://doi.org/10.1029/2000JD900555, 2001.

Freeborn, P. H., M. J. Wooster, W. M. Hao, C. A. Ryan, B. L. Nordgren, S. P. Baker, and C. Ichoku. Relationships between energy release, fuel mass loss, and trace gas and aerosol emissions during laboratory biomass fires, J. Geophys. Res., 113, D01301, doi:10.1029/2007JD008679, 2008.

Ge, C., J. Wang, J. S. Reid, D. Posselt, P. Lynch, E. Hyer, Mesoscale modeling of smoke transport from equatorial Southeast Asian Maritime Continent to the Philippines: First comparison of ensemble analysis with in situ observations, *J. Geophys. Res.- Atmos.*, 122, 5380–5398, 2017.

Gelaro, R., W. McCarty, M.J. Suárez, R. Todling, A. Molod, L. Takacs, C.A. Randles, A. Darmenov, M.G. Bosilovich, R. Reichle, K. Wargan, L. Coy, R. Cullather, C. Draper, S. Akella, V. Buchard, A. Conaty, A.M. da Silva, W. Gu, G. Kim, R. Koster, R. Lucchesi, D. Merkova, J.E. Nielsen, G. Partyka, S. Pawson, W. Putman, M. Rienecker, S.D. Schubert, M. Sienkiewicz, and B. Zhao: The Modern-Era Retrospective Analysis for Research and Applications, Version 2 (MERRA-2). J. Climate, 30, 5419–5454, https://doi.org/10.1175/JCLI-D-16-0758.1, 2017.

Giglio, L., Randerson, J. T., van der Werf, G. R., Kasibhatla, P. S., Collatz, G. J., Morton, D. C., and DeFries, R. S.: Assessing variability and long-term trends in burned area by merging multiple satellite fire products, Biogeosciences, 7, 1171–1186, https://doi.org/10.5194/bg-7-1171-2010, 2010.

Giglio, L., Randerson, J. T., and van der Werf, G. R.: Analysis of daily, monthly, and annual burned area using the fourth-generation global fire emissions database (GFED4), J. Geophys.Res.-Biogeo., 118, 317–328, https://doi.org/10.1002/jgrg.20042, 2013.

Giles, D. M., Sinyuk, A., Sorokin, M. G., Schafer, J. S., Smirnov, A., Slutsker, I., Eck, T. F., Holben, B. N., Lewis, J. R., Campbell, J. R., Welton, E. J., Korkin, S. V., and Lyapustin, A. I.: Advancements in the Aerosol Robotic Network (AERONET) Version 3 database – automated near-real-time quality control algorithm with improved cloud screening for Sun photometer aerosol optical depth (AOD) measurements, Atmos. Meas. Tech., 12, 169-209,https://doi.org/10.5194/amt-12-169-2019, 2019.

Hawbaker, T. J., Radeloff, V. C., Syphard, A. D., Zhu, Z. L., and Steward, S. I.: Detection rates of the MODIS active fire product in the United States. Remote Sens. Environ., 112(5) 2656–2664, 2008.

Hoelzemann, J. J., Schultz, M. G., Brasseur, G. P., Granier, C., and Simon, M.: Global Wildland Fire Emission Model (GWEM): Evaluating the use of global area burnt satellite data, J. Geophys. Res., 109, D14S04, doi:10.1029/2003JD003666, 2004.

Holben, B. N., Eck, T. F., Slutsker, I., Tanre, D., Buis, J. P., Setzer, A., Vermote, E., Reagan, J. A., Kaufman, Y. J., Nakajima, T., Lavenu, F., Jankowiak, I., and Smirnov, A.: AERONET – a federated instrument network and data archive for aerosol characterization, Remote Sens. Environ. 66, 1–16, 1998.

Hyer, E. J., and J. S. Reid. Baseline uncertainties in biomass burning emission models resulting from spatial error in satellite active fire location data, Geophys. Res. Lett., 36, L05802, doi:10.1029/2008GL036767, 2009.

Hyer, E. J., J. S. Reid, and J. Zhang: An over-land aerosol optical depth data set for data assimilation by filtering, correction, and aggregation of MODIS collection 5 optical depth retrievals, Atmos. Meas. Tech., 4, 379–408, doi:10.5194/amt-4-379-2011, 2011.

Ichoku, C., and Ellison, L.Global top-down smoke-aerosol emissions estimation using satellite fire radiative power measurements. Atmospheric Chemistry and Physics, 14(13), 6643-6667. doi:10.5194/acp-14-6643-2014, 2014.

Ichoku, C., Ellison, L. T., Yue, Y., Wang, J., & Kaiser, J. W. Fire and Smoke Remote Sensing and Modeling Uncertainties. Natural Hazard Uncertainty Assessment: Modeling and Decision Support, 215-230, doi: 10.1002/9781119028116.ch14, 2016a.

https://doi.org/10.5194/acp-2019-475
Preprint. Discussion started: 8 July 2019

Ichoku, C., Ellison, L.T., Willmot, K.E., Matsui, T., Dezfuli, A.K., Gatebe, C.K., Wang, J., Wilcox, E.M., Lee, J., Adegoke, J. and Okonkwo, C. Biomass burning, land-cover change, and the hydrological cycle in Northern sub-Saharan Africa. *Environmental Research Letters*, *11*(9), p.095005, 2016b.

Ichoku, C., L. Giglio, M. J. Wooster, and L. A. Remer. Global characterization of biomass-burning patterns using satellite measurements of fire radiative energy. Remote Sensing of Environment, 112 (6): 2950-2962 [10.1016/j.rse.2008.02.009], 2008.

Ichoku, C., R. Kahn, and M. Chin. Satellite contributions to the quantitative characterization of biomass burning for climate modeling, Atmos. Res., 111, 1–28, 2012.

Ichoku, C., and Y. Kaufman. A method to derive smoke emission rates from MODIS fire radiative energy measurements.*IEEE Trans on Geosc & Rem Sens*, **43 (11):** 2636-2649 [10.1109/TGRS.2005.857328], 2005.

Janssens-Maenhout, G., Crippa, M., Guizzardi, D., Dentener, F., Muntean, M., Pouliot, G., Keating, T., Zhang, Q., Kurokawa, J., Wankmüller, R., Denier van der Gon, H., Kuenen, J. J. P., Klimont, Z., Frost, G., Darras, S., Koffi, B., and Li, M.: HTAP_v2.2: a mosaic of regional and global emission grid maps for 2008 and 2010 to study hemispheric transport of air pollution, Atmos. Chem. Phys., 15, 11411–11432, https://doi.org/10.5194/acp-15-11411-2015, 2015.

Kaiser, J. W., Heil, A., Andreae, M. O., Benedetti, A., Chubarova, N., Jones, L., Morcrette, J.-J., Razinger, M., Schultz, M. G., Suttie, M., and van der Werf, G. R.: Biomass burning emissions estimated with a global fire assimilation system based on observations of fire radiative power, Biogeosciences, 9, 527-554, doi:10.5194/bg-9-527-2012, 2012.

Kaiser, J.W., Flemming, J., Schultz, M. G., Suttie, M., andWooster, M. J.: The MACC Global Fire Assimilation System: First Emission Products (GFASv0), Tech. Memo. 596, ECMWF, Reading,UK, 2009.

Kaufman, Y. J., C. O. Justice, L. P. Flynn, J. D. Kendall, E. M. Prins, L. Giglio, D. E. Ward, W. P. Menzel, and A. W. Setzer. Potential global fire monitoring from EOS-MODIS, J. Geophys. Res., 103(D24), 32,215–32,238, doi:10.1029/98JD01644, 1998.

Levy, R.C., Remer, L.A., Kleidman, R.G., Mattoo, S., Ichoku, C., Kahn, R. and Eck, T.F. Global evaluation of the Collection 5 MODIS dark-target aerosol products over land. *Atmospheric Chemistry and Physics*, *10*(21), pp.10399-10420, 2010.

Liousse, B., Guillaume, J. M., Grégoire, M., Mallet, C., Galy, C., Pont, V., Akpo, A., Bedou, M., Castéra, P., Dungall, L., Gardrat, E., Granier, C., Konaré, A., Malavelle, F., Mariscal, A., Mieville, A., Rosset, R., Serça, D., Solmon, F., Tummon, F., Assamoi, E., Yoboué, V., and Van Velthoven, P.: Updated African biomass burning emission inventories in the framework of the AMMAIDAF program, with an evaluation of

https://doi.org/10.5194/acp-2019-475
Preprint. Discussion started: 8 July 2019

combustion aerosols, Atmos. Chem. Phys., 10, 7347–7382, doi:10.5194/acp-10-7347-2010, 2010.

Molod, A. M., L. L. Takacs, M. J. Suarez, and J. Bacmeister. Development of the GEOS atmospheric general circulation model: evolution from MERRA to MERRA2 ." Geosci. Model Dev. 8 1339-1356 [10.5194/gmd-8-1339-2015], 2015.

Pan, X., Chin, M., Gautam, R., Bian, H., Kim, D., Colarco, P. R., Diehl, T. L., Takemura, T., Pozzoli, L., Tsigaridis, K., Bauer, S., and Bellouin, N.: A multi-model evaluation of aerosols over South Asia: common problems and possible causes, Atmos. Chem. Phys., 15, 5903-5928, https://doi.org/10.5194/acp-15-5903-2015, 2015.

Pan, X., Chin, M., Ichoku, C. M., & Field, R. D. Connecting Indonesian fires and drought with the type of El Niño and phase of the Indian Ocean dipole during 1979–2016. Journal of Geophysical Research: Atmospheres, 123. https://doi.org/10.1029/2018JD028402, 2018.

Peterson, D., & Wang, J. A Sub-pixel-based calculate of fire radiative power from MODIS observations: 2. Sensitivity analysis and potential fire weather application. Remote Sensing of Environment, 129, 231–249, 2013.

Peterson, D. A., J. R. Campbell, E. J. Hyer, M. D. Fromm, G. P. Kablick, J. H. Cossuth, and M. T. DeLand. Wildfire-driven thunderstorms cause a volcano-like stratospheric injection of smoke. *npj Climate and Atmospheric Science*, **1,** 30, 2018.

Petrenko, M., R. Kahn, M. Chin, A. Soja, T. Kucsera, and Harshvardhan. The use of satellite-measured aerosol optical depth to constrain biomass burning emissions source strength in the global model GOCART, J. Geophys. Res., 117, D18212, doi:10.1029/2012JD017870, 2012.

Petrenko, M., Kahn, R., Chin, M., & Limbacher, J. Refined use of satellite aerosol optical depth snapshots to constrain biomass burning emissions in the GOCART model. Journal of Geophysical Research: Atmospheres, 122, 10,983–11,004. https://doi.org/10.1002/ 2017JD026693, 2017.

Pereira, G., Siqueira, R., Rosário, N. E., Longo, K. L., Freitas, S. R., Cardozo, F. S., Kaiser, J. W., and Wooster, M. J.: Assessment of fire emission inventories during the South American Biomass Burning Analysis (SAMBBA) experiment, Atmos. Chem. Phys.,16, 6961–6975, doi:10.5194/acp-16-6961-2016, 2016.

Randerson, J. T., Chen, Y., van der Werf, G. R., Rogers, B. M., and Morton, D. C.: Global burned area and biomass burning emissions from small fires, J. Geophys. Res.-Biogeo., 117, G04012, https://doi.org/10.1029/2012JG002128, 2012.

https://doi.org/10.5194/acp-2019-475
Preprint. Discussion started: 8 July 2019

Atmospheric Chemistry and Physics
Discussions

Randles, C. A., A. da Silva, V. Buchard, et al. 2017: The MERRA-2 Aerosol Reanalysis, 1980-onward, Part I: System Description and Data Assimilation Evaluation. J Clim, doi: 10.1175/jclid-16-0609.1

Reddington, C. L., Spracklen, D. V., Artaxo, P., Ridley, D. A., Rizzo, L. V., and Arana, A.: Analysis of particulate emissions from tropical biomass burning using a global aerosol model and long-term surface observations, Atmos. Chem. Phys., 16, 11083-11106, https://doi.org/10.5194/acp-16-11083-2016, 2016.

Remer, L. A., et al. (2005), The MODIS aerosol algorithm, products, andvalidation, J. Atmos. Sci., 62(4), 947–973.

Reid, J. S., R. Koppmann, T. F. Eck, and D. P. Eleuterio. A review of biomass burning emissions part II: Intensive physical properties of biomass burning particles, Atmos. Chem. Phys., 5, 799–825, 2005.

Reid, C.E.; Brauer, M.; Johnston, F.H.; Jerrett, M.; Balmes, J.R.; Elliott, C.T. Critical Review of Health Impacts of Wildfire Smoke Exposure. Environ. Health Perspect, 124, 1334–1343, 2016.

Rienecker, M. M., M. J. Suarez, R. Gelaro, R. Todling, J. Bacmeister, E. Liu, M. G. Bosilovich, S. D. Schubert, L. Takacs, G.-K. Kim, S. Bloom, J. Chen, D. Collins, A. Conaty, A. da Silva, W. Gu, J. Joiner, R. D. Koster, R. Lucchesi, A. Molod, T. Owens, S. Pawson, P. Pegion, C. R. Redder, R. Reichle, F. R. Robertson, A. G. Ruddick, M. Sienkiewicz, J. Woollen, MERRA - NASA's Modern-Era Retrospective Analysis for Research and Applications. J. Climate, 24, 3624–3648, 2011.

Roberts, G., Wooster, M., & Lagoudakis, E. Annual and diurnal African biomass burning temporal dynamics. Biogeosciences, 6, 2009.

Sayer, A. M., L. A. Munchak, N. C. Hsu, R. C. Levy, C. Bettenhausen, and M.-J. Jeong. MODIS Collection 6 aerosol products: Comparison between Aqua's e-Deep Blue, Dark Target, and “merged” data sets, and usage recommendations, *J. Geophys. Res. Atmos.,* 119, 13,965–13,989, doi:10.1002/2014JD022453, 2014.

Simon, H. and Bhave, P. V.: Simulating the Degree of Oxidation in Atmospheric Organic Particles, Environ. Sci. Technol., 46, 331–339, doi:10.1021/es202361w, 2012.

Tansey, K., J. Beston, A. Hoscilo, S. E. Page, and C. U. Paredes Hernandez, Relationship between MODIS fire hotspot count and burned area in a degraded tropical peat swamp forest in Central Kalimantan, Indonesia,J. Geophys. Res.,113, D23112, doi:10.1029/2008JD010717, 2008.

Turpin, B. J. and Lim, H. J.: Species contributions to PM2.5 mass concentrations: Revisiting common assumptions for estimating organic mass, Aerosol Sci. Tech., 35, 602–610, doi:10.1080/02786820152051454, 2001.

https://doi.org/10.5194/acp-2019-475
Preprint. Discussion started: 8 July 2019

van der Werf, G. R., Randerson, J. T., Giglio, L., Collatz, G. J., Kasibhatla, P. S., and Arellano Jr., A. F.: Interannual variability in global biomass burning emissions from 1997 to 2004, Atmos. Chem. Phys., 6, 3423–3441, https://doi.org/10.5194/acp-6-3423-2006, 2006.

van der Werf, G. R., Randerson, J. T., Giglio, L., Collatz, G. J., Mu, M., Kasibhatla, P. S., Morton, D. C., DeFries, R. S., Jin, Y., and van Leeuwen, T. T.: Global fire emissions and the contribution of deforestation, savanna, forest, agricultural, and peat fires (1997–2009), Atmos. Chem. Phys., 10, 11707–11735, https://doi.org/10.5194/acp-10-11707-2010, 2010.

van der Werf, G. R., Randerson, J. T., Giglio, L., van Leeuwen, T. T., Chen, Y., Rogers, B. M., Mu, M., van Marle, M. J. E., Morton, D. C., Collatz, G. J., Yokelson, R. J., and Kasibhatla, P. S.: Global fire emissions estimates during 1997–2016, Earth Syst. Sci. Data, 9, 697-720, https://doi.org/10.5194/essd-9-697-2017, 2017.

van Leeuwen, T. T., van der Werf, G. R., Hoffmann, A. A., Detmers, R. G., Ruecker, G., French, N. H. F., Archibald, S., Carvalho, J. A. J., Cook, G. D., de Groot, W. J., Hely, C., Kasischke, E. S., Kloster, S., McCarty, J. L., Pettinari, M. L., Savadogo, P., Alvarado, E. C., Boschetti, L., Manuri, S., Meyer, C. P., Siegert, F., Trollope, L. A. and Trollope, W. S. W.: Biomass burning fuel consumption rates: a field measurement database, Biogeosciences, 11(24), 7305–7329, doi:10.5194/bg-11-7305-2014, 2014.

van Marle, M. J. E., Kloster, S., Magi, B. I., Marlon, J. R., Daniau, A.-L., Field, R. D., Arneth, A., Forrest, M., Hantson, S., Kehrwald, N. M., Knorr, W., Lasslop, G., Li, F., Mangeon, S., Yue, C., Kaiser, J. W., and van der Werf, G. R.: Historic global biomass burning emissions for CMIP6 (BB4CMIP) based on merging satellite observations with proxies and fire models (1750–2015), Geosci. Model Dev., 10, 3329-3357, https://doi.org/10.5194/gmd-10-3329-2017, 2017.

Wang, J., C. Ge, Z. Yang, E. J. Hyer, J. S. Reid, B.-N. Chew, M. Mahmud, Y. Zhang, and M. Zhang, Mesoscale modeling of smoke transport over the Southeast Asian Maritime Continent: interplay of sea breeze, trade wind, typhoon, and topography, Atmospheric Research, 122, 486-503, doi: 10.1016/j.atmosres.2012.05.009, 2013.

Wang, J., S.A. Christopher, U.S. Nair, J.S. Reid, E.M. Prins, J. Szykman, and J.L. Hand, Mesoscale modeling of Central American smoke transport to the United States, 1: "top-down" assessment of emission strength and diurnal variation impacts, J. Geophys. Res., 11, D05S17, doi:10.1029/2005JD006416, 2006.

Wang, J., Yue, Y., Wang, Y., Ichoku, C., Ellison, L., & Zeng, J. Mitigating satellite-based fire sampling limitations in deriving biomass burning emission rates: Application to WRF-Chem model over the Northern sub-Saharan African Region. Journal of Geophysical Research: Atmospheres, 123, 507–528. https://doi. org/10.1002/2017JD026840, 2018.

https://doi.org/10.5194/acp-2019-475
Preprint. Discussion started: 8 July 2019

Wiedinmyer, C., Akagi, S. K., Yokelson, R. J., Emmons, L. K., Al-Saadi, J. A., Orlando, J. J., and Soja, A. J. The Fire Inventory from NCAR (FINN): a high resolution global model to estimate the emissions from open burning, Geosci. Model Dev., 4, 625–641, doi:10.5194/gmd-4-625-2011, 2011.

Wooster, M. J., B. Zhukov, and D. Oertel. Fire radiative energy for quantitative study of biomass burning: Derivation from the BIRD experimental satellite and comparison to MODIS fire products, Remote Sens. Environ., 86(1), 83–107, doi:10.1016/S0034-4257(03)00070-1, 2003.

Wooster, M. J., G. Roberts, G. L. W. Perry, and Y. J. Kaufman. Retrieval of biomass combustion rates and totals from fire radiative power observations: FRP derivation and calibration relationships between biomass consumption and fire radiative energy release, J. Geophys. Res., 110, D24311, doi:10.1029/2005JD006318, 2005.

Yang, Z., J. Wang, C. Ichoku, E. Hyer, and J. Zeng, Mesoscale modeling and satellite observation of transport and mixing of smoke and dust particles over northern sub-Saharan African region, J. Geophys. Res. Atmos., 118, 12,139-12,157, doi:10.1002/2013JD020644, 2013.

Yokelson, R. J., Burling, I. R., Urbanski, S. P., Atlas, E. L., Adachi, K., Buseck, P. R., Wiedinmyer, C., Akagi, S. K., Toohey, D. W., and Wold, C. E.: Trace gas and particle emissions from open biomass burning in Mexico, Atmos. Chem. Phys., 11, 6787–6808, doi:10.5194/acp-11-6787-2011, 2011.

Zhang, F., J. Wang, C. M. Ichoku, et al.. Sensitivity of mesoscale modeling of smoke direct radiative effect to the emission inventory: a case study in northern sub-Saharan African region. Environmental Research Letters, 9 (7): 075002 (14 pp) [10.1088/1748-9326/9/7/075002], 2014.

Zhu, J., X. Xia, J. Wang, C. Wiedinmyer, J. A. Fisher, C. A. Keller. Impact of Southeast Asian smoke on aerosol properties in Southwest China: first comparison of model simulations with satellite and ground observation, J. Geophys. Res.-Atmos., 122, 3904–3919, 2017.

https://doi.org/10.5194/acp-2019-475
Preprint. Discussion started: 8 July 2019

Atmospheric Chemistry and Physics
Discussions
Open Access
EGU

FIGURES

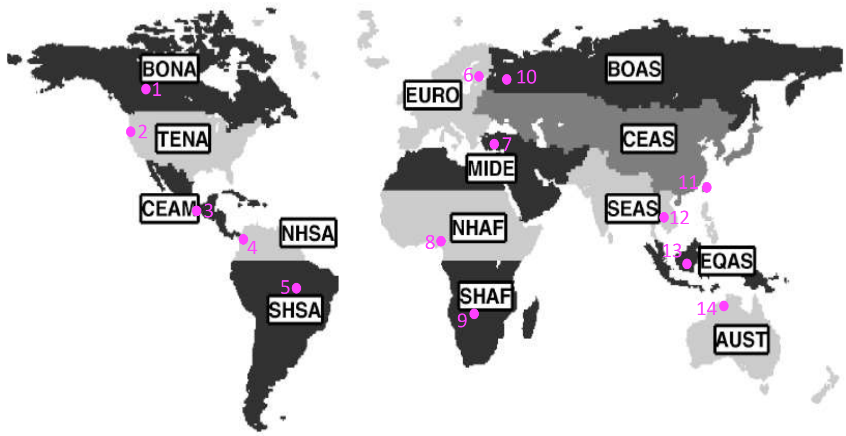

BONA	Boreal North America	NHAF	Northern Hemisphere Africa
TENA	Temperate North America	SHAF	Southern Hemisphere Africa
CEAM	Central America	BOAS	Boreal Asia
NHSA	Northern Hemisphere South America	CEAS	Central Asia
SHSA	Southern Hemisphere South America	SEAS	Southeast Asia
EURO	Europe	EQAS	Equatorial Asia
MIDE	Middle East	AUST	Australia and New Zealand

Figure 1. Map showing the 14 regions used in this study, following GFED regionalization defined by Giglio et al. (2006) and van der Werf et al. (2006; 2017). The fourteen AERONET sites selected for detailed analysis in the respective regions are represented by the numbered magenta dots. These AERONET sites and the included data years (in parentheses) for calculating aerosol climatology are: 1-Fort McMurray (2005-2018), 2-Monterey (2002-2018), 3-Tuxtla Gutierrez (2005-2010), 4-Medellin (2012-2016), 5-Alta Floresta (1993-2018), 6-Toravere (2002-2017), 7-IMS METU ERDEMLI (1999-2017), 8-Ilorin (1998-2018), 9-Mongu (1997-2010), 10-Moscow MSU MO (2001-2017), 11-EPA NCU (2004-2018), 12-Chiang Mai Met Sta (2007-2017), 13-Palangkaraya (2012-2017), 14-Lake Argyle (2001-2017).

https://doi.org/10.5194/acp-2019-475
Preprint. Discussion started: 8 July 2019

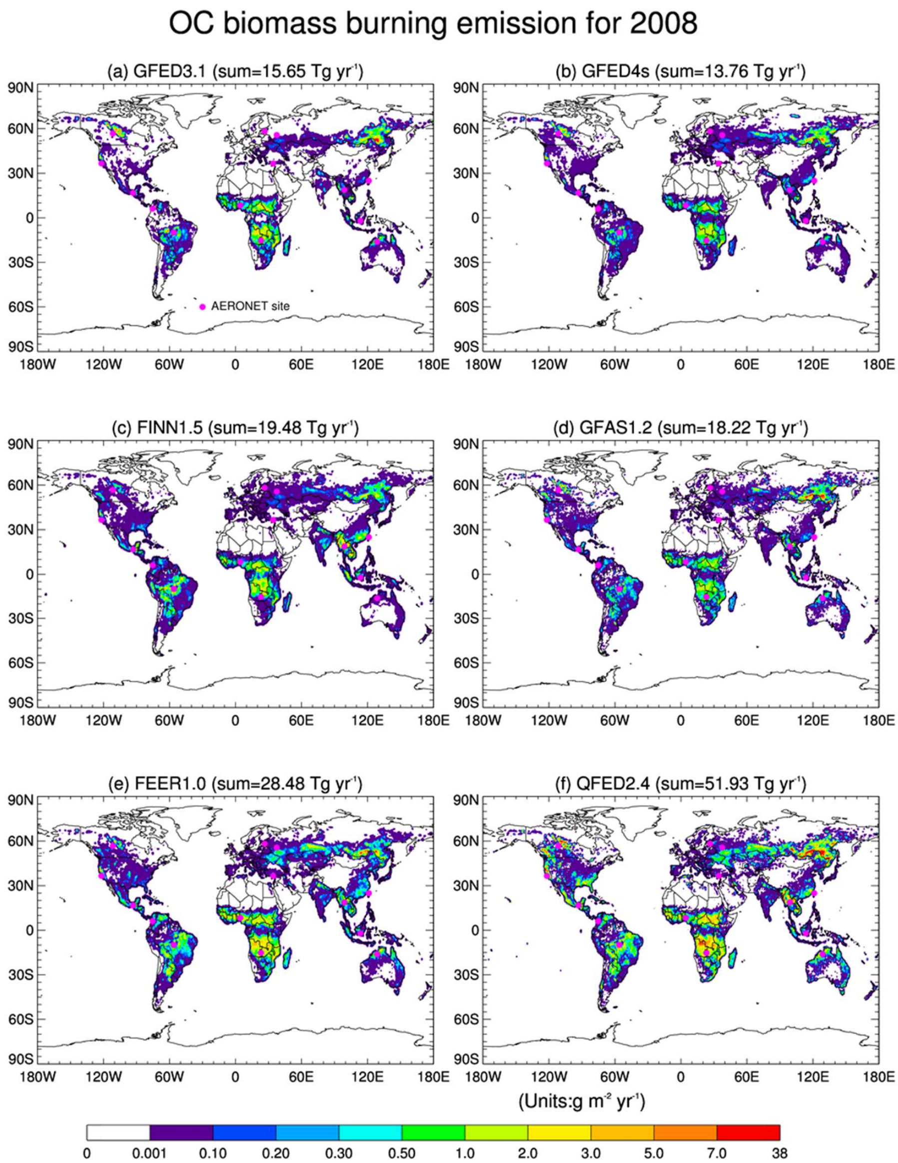

Figure 2. The spatial distribution of annual organic carbon biomass burning emissions for 2008 estimated by six biomass burning emission datasets. The fourteen selected AERONET sites are indicated as magenta dots.

https://doi.org/10.5194/acp-2019-475
Preprint. Discussion started: 8 July 2019

Atmospheric Chemistry and Physics
Discussions

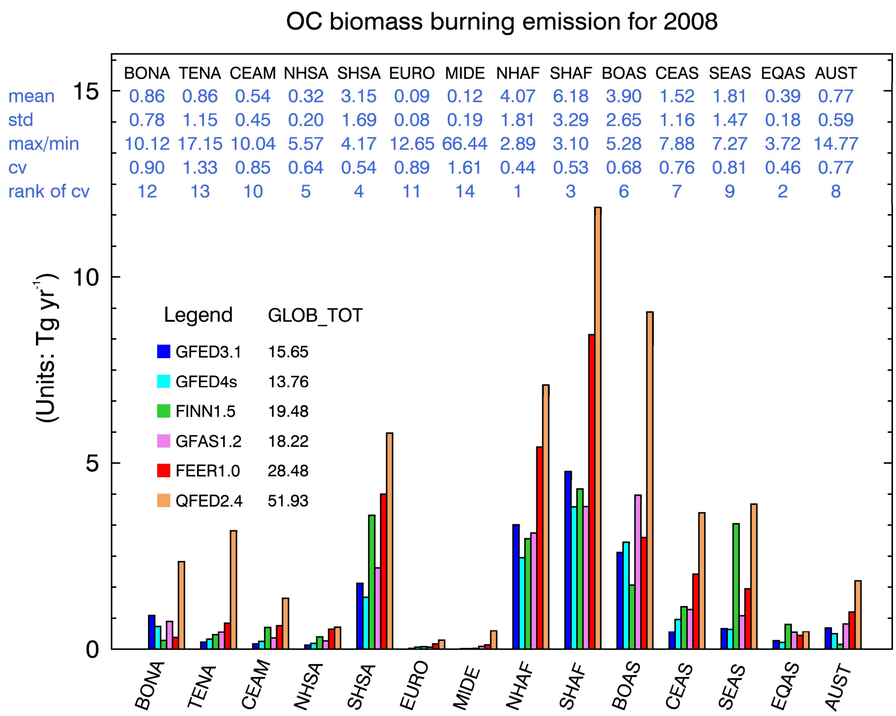

Figure 3. The regional total annual organic carbon biomass burning emissions for 2008 in six biomass burning emission datasets (units: Tg yr-[1]). Relevant statistics for the six BB emission datasets in each region are also listed under the short name of each region on the top of the panel in blue, with the mean of the six BB emission datasets in the first row. Three different methods to measure the spread of the six BB emission datasets are shown as well: one absolute method, i.e., the standard deviation (std) in the second row, and two relative methods, i.e., the ratio of max to min (i.e., maximum/minimum) shown in the third row, and the coefficient of variation (cv), defined as the ratio of the std to the mean, in the fourth row. The rankings of the regions regarding the spread of the BB emissions datasets according to cv are shown in the fifth row (i.e., a ranking of 1 means that this region shows the least spread among the six BB emissions datasets, while a ranking of 14 indicates that this region has the largest spread among the 14 regions).

https://doi.org/10.5194/acp-2019-475
Preprint. Discussion started: 8 July 2019

Atmospheric Chemistry and Physics
Discussions

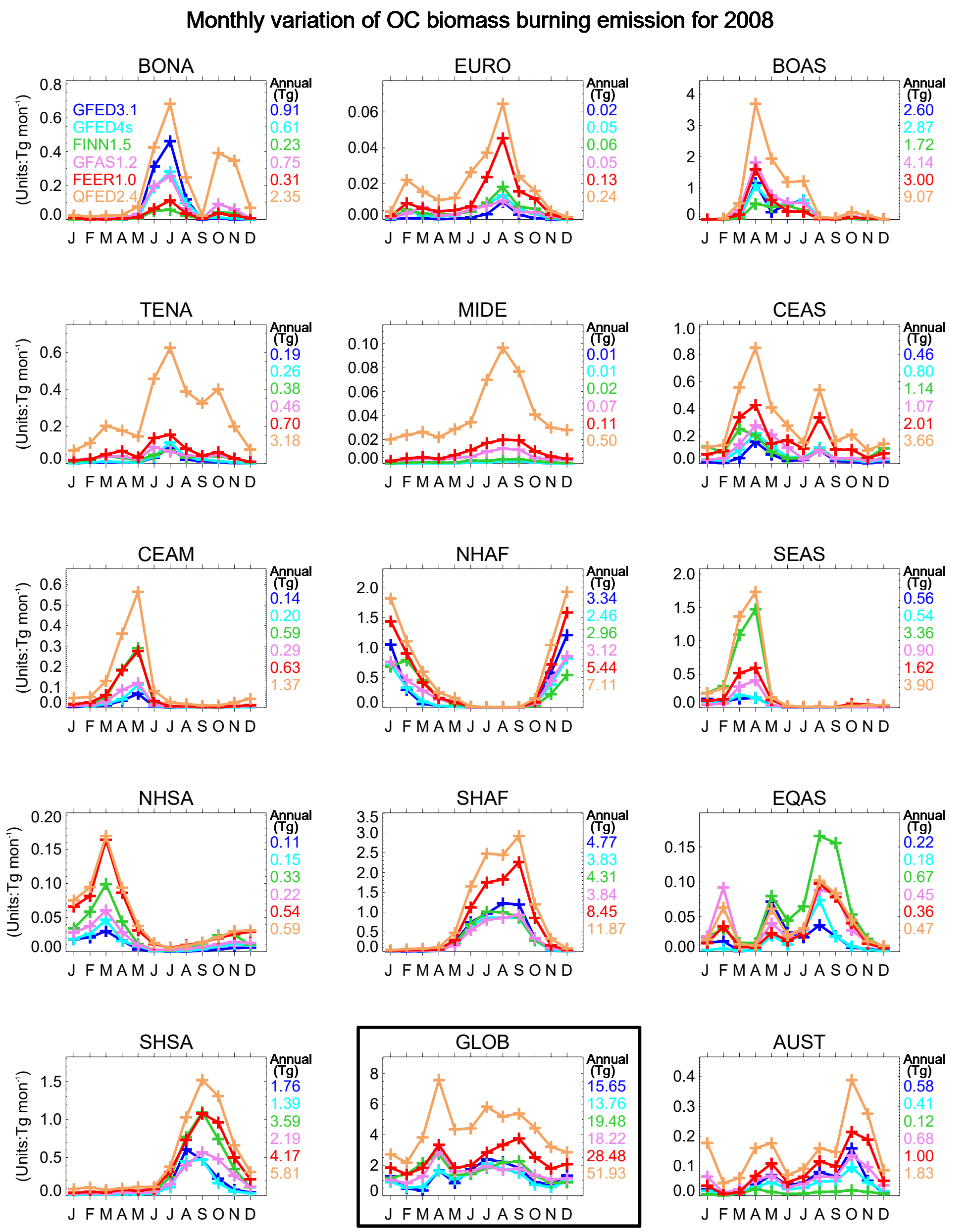

Figure 4. Monthly variation of organic carbon biomass burning emissions for 2008 in six biomass burning emission datasets in 14 regions and the globally (i.e., GLOB, highlighted with a black box). The total annual emission is listed on the right side of each panel.

https://doi.org/10.5194/acp-2019-475
Preprint. Discussion started: 8 July 2019

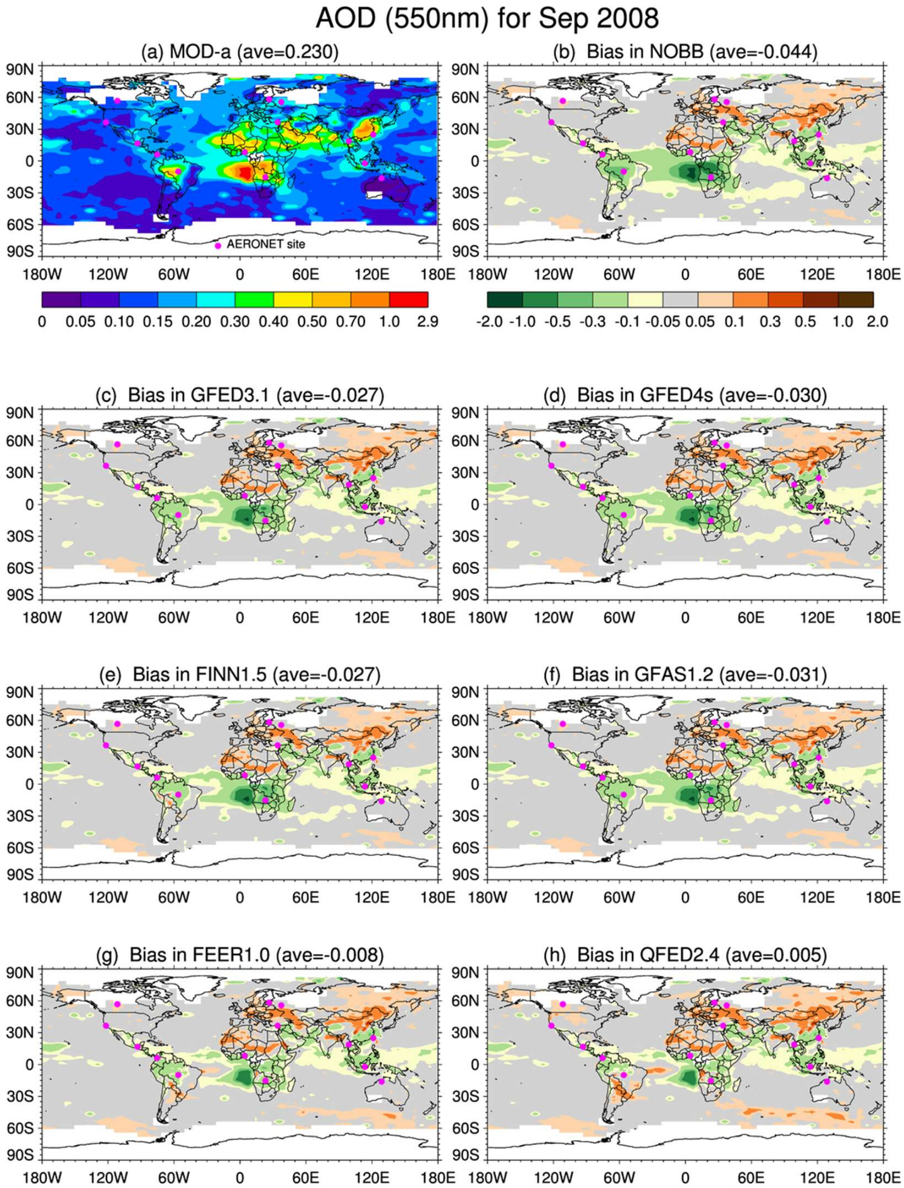

Figure 5. (a) The spatial distribution of monthly mean AOD at 550nm for September 2008 from MODIS-aqua (i.e., MOD-a) with the white color representing missing value. The global averaged value (ave) is shown in the parentheses. The fourteen selected AERONET stations are labeled as magenta dots. (b)-(h) are for GEOS model biases (i.e., model minus MODIS-a) in seven model experiments, i.e., bias in (b) NOBB, (c) GFED3.1, (d) GFED4s, (e) FINN1.5, (f) GFAS1.2, (g) FEER1.0, (h) QFED2.4, respectively.

https://doi.org/10.5194/acp-2019-475
Preprint. Discussion started: 8 July 2019

Atmospheric Chemistry and Physics
Discussions

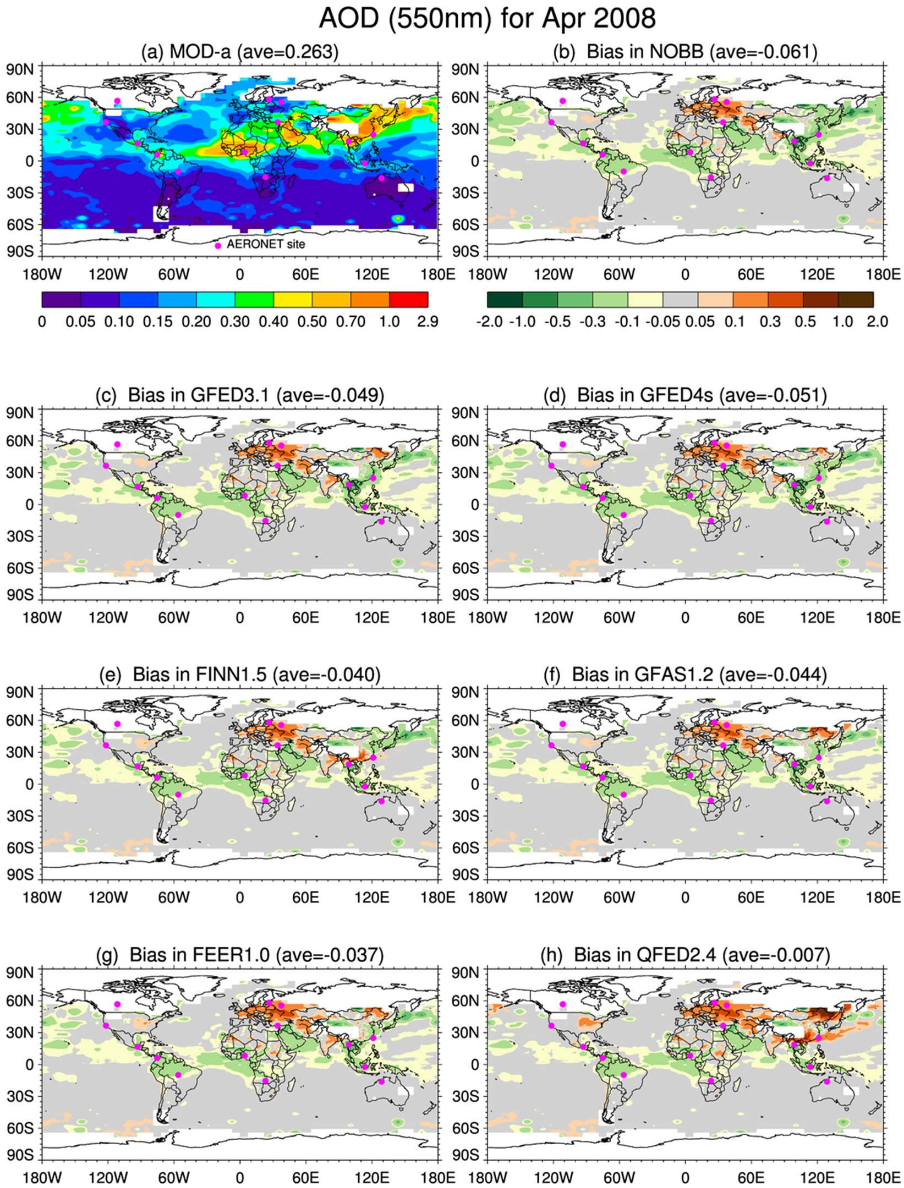

1285
1286 Figure 6. Same as Figure 5 except for April 2008.
1287

https://doi.org/10.5194/acp-2019-475
Preprint. Discussion started: 8 July 2019

Atmospheric Chemistry and Physics
Discussions

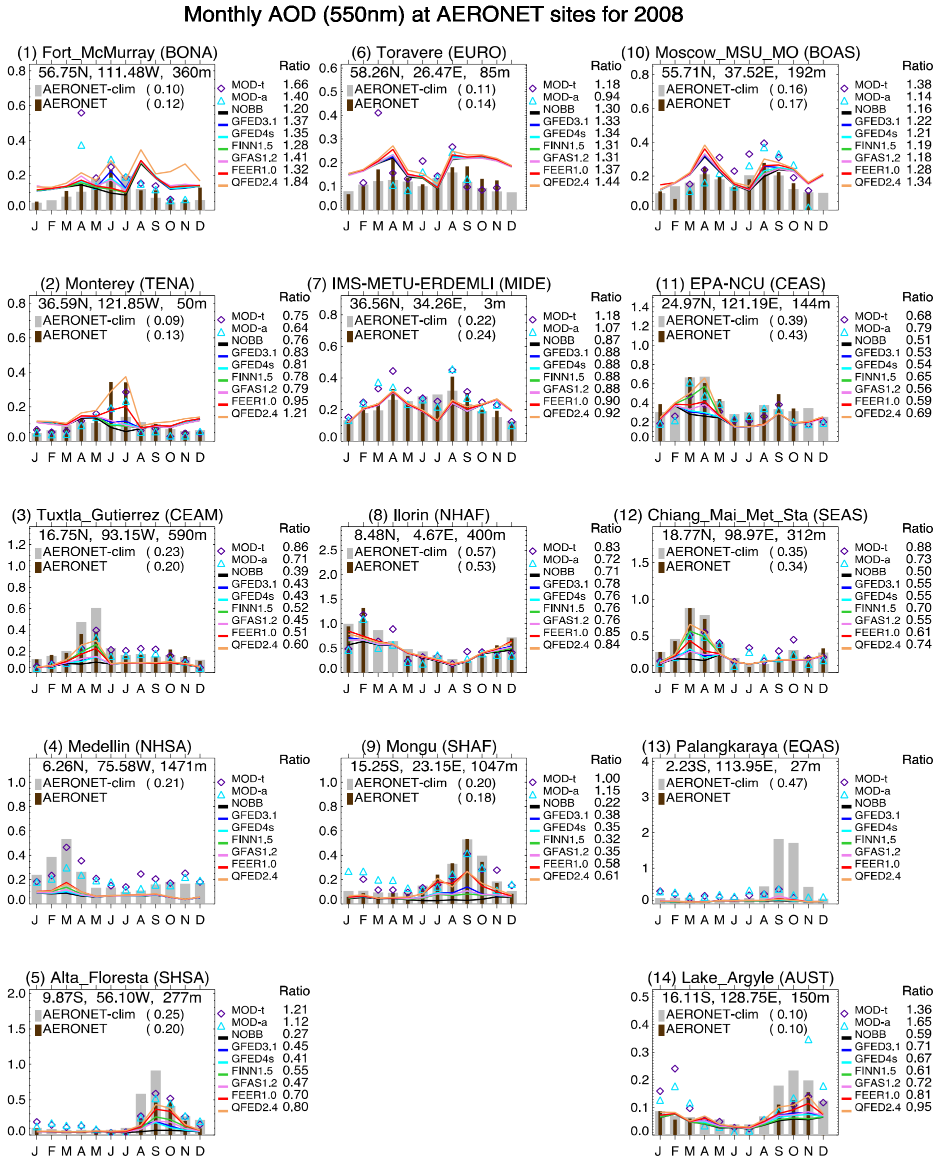

Figure 7. Monthly variation of AOD (at 550nm wavelength) for 2008 over 14 AERONET sites selected from their respective regions, as indicated in parentheses. The climatology of AERONET AOD is represented by light gray thick bars with yearly mean value shown in the parenthesis after its name, along with the monthly AERONET AOD represented by brown thin bars. MODIS-Terra (MOD-t), MODIS-Aqua (MOD-a) are purple diamond and blue triangle, respectively, and seven GEOS experiments with different biomass burning emission options are represented in different line colors. The annual ratio (model/AERONET) listed on the right hand is estimated by averaging over monthly ratio.

Atmospheric Chemistry and Physics
Open Access
EGU
Discussions

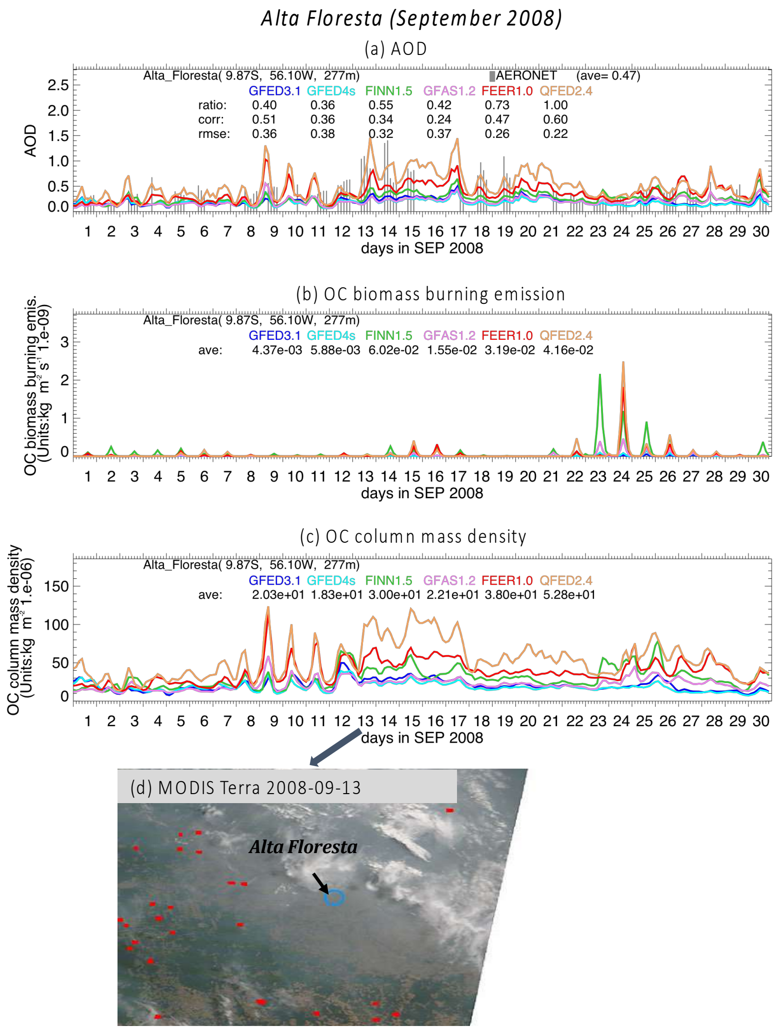

Figure 8. Characteristics of the observed and the simulated aerosols at Alta Floresta during September 2008: (a) The 3-hourly time series of AOD at 550nm. The AERONET is represented by vertical gray bars, and the outputs from the six model experiments are represented by the color curves. The relevant statistics are listed: *ave* is the monthly average, *ratio* is the fraction of the simulated to the observed AOD at all observed hours, *corr* is correlation between the observed and the simulated AOD, and *rmse* is root mean square error. (b) The 3-hourly time series of local biomass burning OC emission rate averaged over the grid box where Alta Floresta is located. (c) Same as (b) but OC column mass density. (d) MODIS-Terra true color image near and at Alta Floresta on September 13, 2008, overlaid with the active fire hot spots in red dots (Image credit: https://aeronet.gsfc.nasa.gov/cgi-bin/bamgomas_interactive and https://worldview.earthdata.nasa.gov).

https://doi.org/10.5194/acp-2019-475
Preprint. Discussion started: 8 July 2019

Atmospheric Chemistry and Physics
Open Access
Discussions
EGU

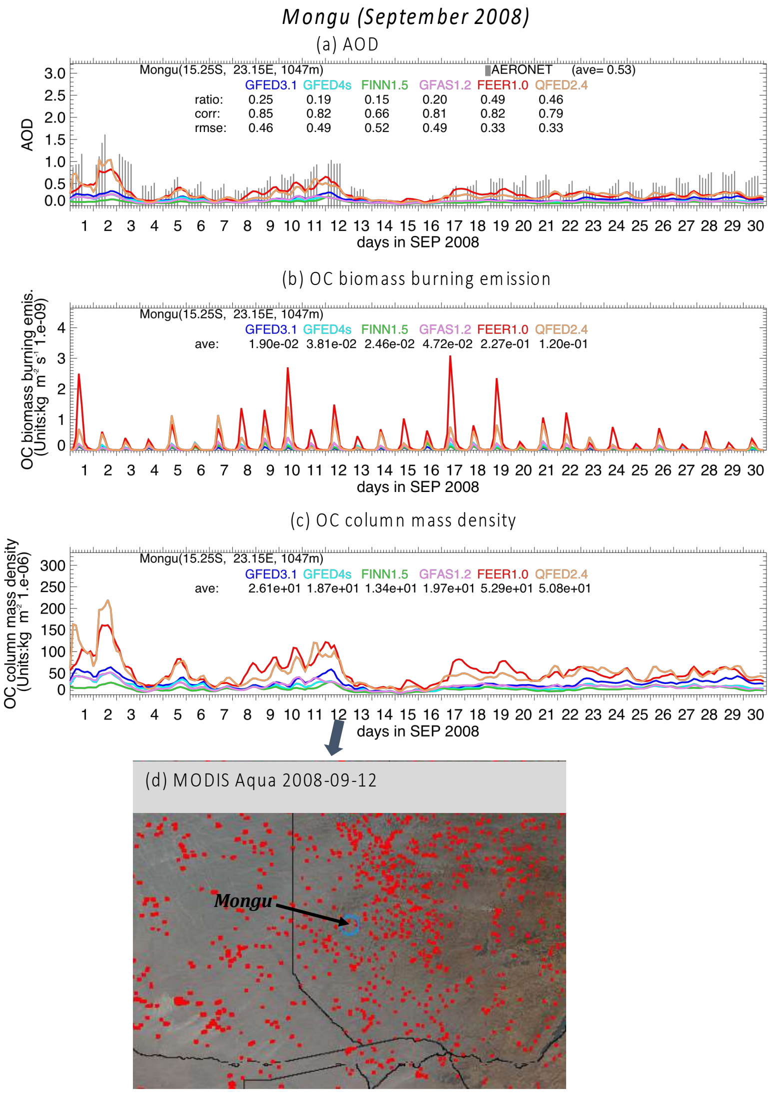

Figure 9. Characteristics of the observed and the simulated aerosols at Mongu during September 2008: (a) The 3-hourly time series of AOD at 550nm. The AERONET is represented by vertical gray bars, and the outputs from the six model experiments are represented by the color curves. The relevant statistics are listed: *ave* is the monthly average, *ratio* is the fraction of the simulated to the observed AOD at all observed hours, *corr* is correlation between the observed and the simulated AOD, and *rmse* is root mean square error. (b) The 3-hourly time series of local biomass burning OC emission rate averaged over one grid box where Mongu is located. (c) Same as (b) but OC column mass density. (d) MODIS-Aqua true color image near and at Mongu on September 12, 2008, overlaid with the active fire hot spots in red dots (Image credit: https://aeronet.gsfc.nasa.gov/cgi-bin/bamgomas_interactive and https://worldview.earthdata.nasa.gov).

https://doi.org/10.5194/acp-2019-475
Preprint. Discussion started: 8 July 2019

Table 1. Summary of six biomass burning emission datasets during MODIS-era (i.e., 2000-present)

a. Burned area based approaches

BB Emission Dataset	Original Grid	Time-Frame/ Frequency	Burned Area	Active Fire Product	Fuel Consumption	Emission Factor
GFED3.1	0.5°×0.5° (lon×lat)	2000-2012/ 3-hourly, daily, monthly	MOD09GHK and/or MYD09GHK	Gridded composite L3 fire product MOD14A1 and/or MYD14A1	Estimated in CASA by product of fuel load and combustion completeness	Mainly from Andreae and Merlet (2001) with annual updates
GFED4s	0.25°×0.25° (lon×lat)	2000-2016/ 3-hourly, daily, monthly	Daily MCD64A1 product in Collection 5.1 at 500m spatial resolution	L3 MOD14A1 and MYD14A1; fire location product MCD14ML	Revised CASA by optimizing parameterization, reorientation of fuel consumption in frequently burned landscapes	Mainly from Akagi et al. (2011), supplemented by Andreae and Merlet (2001) and other
FINN1.5	1km^2	2002-2015/ daily	Estimated by active fire counts: 0.75 km^2 for savannas at each fire pixel, 1km^2 for other types	MODIS NRT active fire product (MCD14DL)	Assigned according to the global wildland fire emission model (Hoelzemann et al., 2004) with updates	Mainly from Andreae and Merlet (2001) and Akagi et al. (2011), with updates through 2015

b. FRP based approaches

BB Emission Dataset	Original Grid	Time-Frame/ Frequency	FRP	Emission Coefficient (C_e)	Emission Factor
GFAS1.2	0.1×0.1 (lon×lat)	2003-Present/daily	Assimilation of level 2 MOD14 and MYD14 FRP	Calculated by regression of FRP to dry matter combustion rate of GFED v3.1 in 8 biomes.	Mainly from Andreae and Merlet (2001) with updates from literatures through 2009
FEER1.0	0.1×0.1 (lon×lat)	2003-Present/ daily, monthly	From GFASv1.2 (Kaiser et al., 2012, see above)	Calculated by linear regression between FRP and total particulate matter emission rate estimated from MODIS AOD at each grid	Andreae and Merlet (2001) with updates provided by Andreae in 2014
QFED2.4	0.1×0.1 (lon×lat)	2000-Present/ daily, monthly	Level 2 fire products MOD14/MYD14	Calculated by regression of the GEOS simulated AOD to the MODIS AOD in 46 sub-regions and then aggregated into 4 biome.	Andreae and Merlet (2001)

LCT: land cover type
VCF: Vegetation continuous fields
CASA: Carnegie-Ames-Stanford-Approach biogeochemical

https://doi.org/10.5194/acp-2019-475
Preprint. Discussion started: 8 July 2019

Table 2. Comparison of emission factor (Units: g species per kg dry matter burned) used by GFED3.1[1] and GFED4s[2] (listed in the upper and lower part of the cell respectively, bold if GFED4s is larger).

	Savanna and Grassland	Tropical Forest	Temperate Forest [3]	Boreal forest [3]	Peat Fires [4]	Agricultural Residues
OC	3.21	4.30	9.14	9.14	4.30	3.71
	2.62	**4.71**	**9.60**	**9.60**	**6.02**	2.30
BC	0.46	0.57	0.56	0.56	0.57	0.48
	0.37	0.52	0.50	0.50	0.04	**0.75**
SO_2	0.37	0.71	1.00	1.00	0.71	0.40
	0.48	**0.40**	**1.10**	**1.10**	0.40	0.40
CO_2	1646	1626	1572	1572	1703	1452
	1686	**1643**	**1647**	1489	1703	**1585**
CO	61	101	106	106	210	94
	63	93	88	**127**	210	**102**

1. Mainly from Andreae and Merlet (2001) with annual updates
2. Mainly from Akagi et al. (2011), supplemented by Andreae and Merlet (2001) and other sources
3. GFED4s (van der Werf et al., 2017) further divides extra-tropical forest in GFED3 (van der Werf et al., 2010) into temperate forest and boreal forest.
4. Based on Christian et al. (2003) for CO_2, and CO.